

# Weak mean flows induced by anisotropic turbulence impinging onto planar and undulating surfaces

By K. NAGATA<sup>1</sup>, H. WONG<sup>2†</sup>, J. C. R. HUNT<sup>3</sup>,  
S. G. SAJJADI<sup>4</sup> AND P. A. DAVIDSON<sup>5</sup>

<sup>1</sup>Department of Mechanical Science and Engineering,  
Nagoya University, Nagoya 464-8603, Japan

<sup>2</sup>Department of Applied Mathematics and Theoretical Physics,  
University of Cambridge, Cambridge CB3 9EW, UK

<sup>3</sup>Department of Space and Climate Physics and Department of Earth Science,  
University College London, London WC1E 6BT, UK and J. M. Burgers Center,  
University of Technology, Delft, Netherlands

<sup>4</sup>Department of Mathematics, Embry-Riddle Aeronautical University,  
600 S. Clyde Morris Blvd, Daytona Beach, FL 32114-3900, USA

<sup>5</sup>Department of Engineering, University of Cambridge, Cambridge CB2 1PZ, UK

(Received 22 July 2004 and in revised form 23 November 2005)

Prandtl's secondary mean motions of the second kind are driven by the variation of Reynolds stresses near resistive boundaries. In the flows considered here the turbulence is generated away from the boundary in the absence of a mean flow and then impacts onto a rigid surface placed into the flow at  $t=0$ . The initial development of the distorted flow is obtained using the linear approximation and the statistical analysis of rapid distortion theory, following Hunt & Graham (1978) assuming homogeneous stationary high-Reynolds-number turbulence with an integral length scale  $L_\infty$  and r.m.s. velocity  $v'_\infty$ . First, the effects of axisymmetric anisotropy and of different forms of the spectra are analysed for turbulence impinging onto a plane surface lying at an angle  $\alpha$  to the unit vector  $\mathbf{e}$  of the axis of symmetry of the energy spectrum tensor  $\Phi_{ij}(\mathbf{k})$ .  $R$  is defined as the ratio of the largest to smallest variances of the velocity components. The surface blocking leads to gradients of Reynolds shear stresses normal to the surface in the source layer  $B^{(s)}$  with thickness of order  $L_\infty$  and thence to a mean velocity  $U(t) \sim -tv'_\infty^2 \sin 2\alpha(1 - 1/R)/L_\infty$  along the slope in the opposite direction of the projection of  $\mathbf{e}$  onto the plane (i.e. in the direction  $(\mathbf{e} \wedge \mathbf{n}) \wedge \mathbf{n}$  where  $\mathbf{n}$  is the normal into the flow).  $U$  is greatest near the surface where  $y \ll L_\infty$ . As a result of shear stresses being induced by the mean velocity gradient, a steady flow results over a time scale  $T_L = L_\infty/v'_\infty$  – an order of magnitude estimate for the steady-state mean velocity is thence  $U(t/T_L \rightarrow \infty) \sim v'_\infty(\sin 2\alpha(1 - 1/R))^{1/2}$ . Secondly, the effect of a curved surface is studied by analysing isotropic turbulence near an undulating surface of wavelength  $\Lambda$  and amplitude  $H$ , with a low slope so that  $H \ll \Lambda$ . The boundary condition of zero normal velocity at the curved surface generates larger irrotational fluctuations in the troughs, smaller fluctuations over the crest, and shear stresses over the slopes. The curl of the gradients of Reynolds normal and shear stresses within  $B^{(s)}$  cause the growth of a mean vorticity which induces a mean velocity of order  $-tv'_\infty^2/L_\infty$  within  $B^{(s)}$  and a weaker recirculating velocity of order  $-tv'_\infty^2/\Lambda$  in a deeper wave

† Present address: European Space Agency and AOES, Haagse Schouwweg 6G, Leiden, Netherlands.

layer,  $B^{(w)}$ , with thickness of order  $\Lambda$  outside  $B^{(s)}$ . The wavelength of the mean motion is  $\Lambda$ , with downward motions over the troughs and upward motion over the crest. As in the first case, a steady flow is predicted when  $t/T_L \gg 1$ . Anisotropic free-stream turbulence also induces mean motions on undulating surfaces with the same wavelength  $\Lambda$  as that of the undulating surface, but the directions of these mean motions can be towards or away from the troughs/crests depending on the orientation of the anisotropy of the free stream. Flow visualization experiments conducted in a mixing box with oscillating anisotropic and isotropic grids demonstrated the existence of these mean flows and that they reach a steady state with an intensity and length scale comparable to those predicted. These results are also consistent with numerical simulation of Krettenauer & Schumann (1992) of convective turbulence over an undulating surface.

---

## 1. Introduction

In turbulent flows near rigid (or deformable) surfaces, the fluctuating velocity field (having an r.m.s. value  $v'_{\infty}$ ) is either generated locally, by mean velocity gradients and by body forces, or is transported there by the mean flow and by self-induced motions of the eddies, e.g. from an oscillating grid or a shear layer above the surface (Wood & Bradshaw 1984). However, the structure of the turbulence is also affected by the direct effects of the kinematic conditions at the surface, i.e. the parallel and normal components of the velocity should be zero (or match those of the surface). The effects of these boundary conditions on production, eddy transport and dissipation are usually not applied explicitly in most one-point statistical models of shear flows. Some account is taken of the elliptic effects in auxiliary models or in modelling wall functions (e.g. Gibson & Launder 1978; Durbin 1993). In turbulent shear-free flows such as thermal convection (e.g. Plate *et al.* 1998) they are essential in determining the eddy structure and other properties of the flow such as heat flux. As this paper shows, when the free-stream turbulence is anisotropic, the non-uniform gradients of the turbulence near a planar surface can induce gradients of Reynolds stress, so that an initially shear free flow becomes a sheared turbulent flow.

What happens to the turbulence and the mean flow if the surface is not planar and there are non-uniformities at the surface? Prandtl (1956) explained how the spatial variations of Reynolds stresses  $\partial(\overline{u_i u_j})/\partial x_j$  (where  $u_i$  is the fluctuating velocity), generated in unidirectional shear flows  $U_1(y, z)$  over general non-planar surfaces that are aligned with the mean flow ( $y = y_s(z)$ ), could force weak mean flows with mean velocity components ( $U_2, U_3$ ), of order  $v'_{\infty}$ , such as those directed into and out of the corner regions of rectangular ducts. He called these 'secondary motions of the second kind' to distinguish them from those of the 'first' kind driven by normal pressure gradients driven by curvature of the mean flow such as occurs in pipe bends. These flows generated in the corner of two plates perpendicular to each other placed in an oncoming turbulent flow were one of the test cases for turbulent models at Stanford in 1980 (Gessner & Emery 1981).

Previous calculations of these secondary flows have been based on turbulence model equations relating the gradients of the mean velocity  $\partial U_i/\partial x_j$  to the second moments of the turbulence  $\overline{u_i u_m}$  (Launder & Ying 1972; Townsend 1976). However, no allowance was made for Reynolds stress gradients caused by the direct impingement of the large eddies onto the surface, which are particularly important in 'shear free'

turbulent flows where the turbulence intensity is large relative to any variations in the mean velocity near the surface  $\Delta U$ , i.e.  $v'_{\infty}/\Delta U \gg 1$ . Such flows occur in thermal convection, near free surfaces and in boundary layers with intense large-scale free-stream turbulence. So far, the structures of these shear-free turbulent flows have only been studied theoretically, experimentally and numerically for approximately isotropic turbulence near planar surfaces (Thomas & Hancock 1977; Hunt & Graham 1978 (hereinafter HG); Hunt 1984; Perot & Moin 1995; Kit, Strang & Fernando 1997).

In this paper, we extend the method of rapid distortion theory for inhomogeneous turbulence to analyse the distortion of initially homogeneous turbulence when a sloping or undulating surface  $y = y_s(x, z)$  (where  $v'_{\infty}/\Delta U \gg 1$ ) is introduced at  $t = 0$ . First, we extend the analysis of HG to the case where the undistorted turbulence is anisotropic with principal axes that are not parallel to the plane and for the surface to be undulating. We consider axisymmetric turbulence in the free stream using the ansatz of Sreenivasan & Narasimha (1978) to define the three-dimensional energy spectrum tensor  $\Phi_{\infty ij}$  in the free stream. Solutions are obtained for the flat-plate problem by taking a form of energy spectrum  $E(K) \propto K^4 \exp(-K^2)$  (where  $K$  is the normalized wavenumber) that occurs in many laboratory turbulent flows and in direct numerical simulations (Townsend 1976). This form of spectrum is simpler to analyse than the von Kármán form used by HG. We assume the Reynolds number of the energy-containing eddies  $v'_{\infty} L_{\infty}/\nu$  is large, where  $\nu$  is the kinematic viscosity of the fluid. Note that the main contribution to the distorted turbulent stresses comes from the large-scale eddies and is largely independent of the small-scale spectra. Spectra, variances and cross-correlations are calculated near plane and wavy surfaces and are used to derive expressions for the Reynolds stresses. Over a curved surface, the strengths of these 'sources' of vertical motions are affected by the horizontal components of the free-stream fluctuation. The gradients of the Reynolds stresses (both normal and shear stresses) induce a mean rotational motion. Townsend (1976) showed how such gradients at the edge of a boundary layer on a flat plate produce a mean secondary flow with velocity field  $\mathbf{U}$ , driven by the sharp change in surface conditions. Over a plane, the mean velocity is confined to a boundary layer with thickness of the order of  $L_{\infty}$ . For turbulence over an undulating surface, the perturbations of the turbulence vary over horizontal distances of order  $\Lambda$ . It is assumed that  $\Lambda \gg L_{\infty}$ . Our analysis shows that this leads to the mean flow varying over a scale  $\Lambda$  normal to the surface.

The theory for the turbulence distortion is strictly valid as a small time expansion when  $t \leq T_L = L_{\infty}/v'_{\infty}$ ; but, as with other calculations of rapid distortion theory, when the distortion leads to slow changes of turbulence with time, the theory has been found to describe the main features of the flow even when  $t \gg T_L$  (Hunt & Carruthers 1990). A nonlinear analysis supports this conjecture when there is no mean flow (Magnaudet 2003). For both the particular inhomogeneous turbulent velocity fields considered here, the curl of the gradients of the mean Reynolds stress is non-zero causing the mean vorticity  $\Omega_z(x, y, t)$  to grow with time, but the form of the mean vorticity profile varies slowly because the turbulence structure is slowly varying. Thence the weak secondary mean velocity field with components  $U_1(x, y, t)$ ,  $U_2(x, y, t)$  is calculated. When the mean vorticity becomes comparable with  $v'_{\infty}/L_{\infty}$ , nonlinear effects are significant and the linear analysis becomes invalid.

The fact that  $\Omega_z$  grows when shear-free anisotropic turbulence impinges onto a *plane* surface has not apparently been studied or even proposed before. This mechanism operates within many types of shear flow where large-scale turbulence impinges on a rigid surface, for example in separated or other kinds of free shear

layers which reattach or move close to a rigid surface (e.g. Wood & Bradshaw 1984). Hunt & Morrison (2000) and Högström, Hunt & Smedman (2002) showed that this ‘blocking’ effect contributes significantly to the shear stresses in the surface layer of turbulent boundary layers. Over an undulating surface, if the free-stream turbulence is anisotropic, this planar blocking mechanism operates in addition to the curvature blocking mechanism. It is not generally realized that both mechanisms contribute to the mean motions that are also driven by convective turbulence over an undulating surface (Krettenauer & Schumann 1992), where thermal convection produces anisotropic turbulence over a curved surface. The barotropic mechanisms explained in this paper also affect the convectively driven turbulence and contribute to the mean flow. The importance of such mean motions on the formation of undulations on erodible surfaces has been established (e.g. Bagnold 1941; Feltham, Worster & Wettlaufer 2002) though the effects of large-scale turbulence on the process have not previously been studied.

Mean flow generation by anisotropic velocity fluctuations has been observed in turbulent thermal convection (Krishnamurti & Howard 1981; Owinoh *et al.* 2004) and in mixing boxes (e.g. McDougall 1979; Fernando & de Silva 1993). In fact it is quite difficult to produce anisotropic inhomogeneous turbulence without also generating a mean flow, for the reasons demonstrated in this paper. These flow structures are manifestations of the broad class of large-scale phenomena driven by small-scale anisotropic and inhomogeneous fluctuation that are found in most complex media governed by physical, chemical or biological processes (e.g. Prigogine & Stengers 1984). At present there are no general theories, and detailed calculations are required in each case.

Experiments to test these ideas were performed in a mixing box with an oscillating grid for both the plane surface and undulating surface. Their results, described in sections §§ 6.1 and 6.2, respectively, are in good qualitative agreement with the theoretical results. For fuller details of these experiments, see Wong (1985).

## 2. Linear analysis of distorted anisotropic turbulence and the mean flow field

### 2.1. Equations and orders of magnitude

Consider the flow depicted in figure 1, in which homogeneous, statistically stationary (not necessarily isotropic) turbulence  $\mathbf{u}_\infty^*(\mathbf{x}, t)$  with no mean flow, such as might be generated by a grid at  $y = y_g$ . A fixed rigid surface  $y = y_s(x, z)$  is introduced into the flow when  $t > 0$ . The solution procedures are developed from those of Hunt & Graham (1978). (They considered flow with a uniform mean velocity  $\bar{u}_\infty$  and showed that the effects of the initial upstream condition do not persist downstream.) For the different kind of turbulence considered here, the mean velocity field  $\mathbf{U}(\mathbf{x}, t)$  is initially zero, but then grows with time.

The mean and fluctuating components of the velocity, pressure and vorticity fields are  $\hat{\mathbf{u}} = \mathbf{U}^* + \mathbf{u}^*$ ,  $\hat{p} = P^* + p^*$ ,  $\hat{\boldsymbol{\omega}} = \boldsymbol{\Omega}^* + \boldsymbol{\omega}^*$ , where  $\hat{\mathbf{u}} = \mathbf{U}^*$ ,  $\hat{\boldsymbol{\omega}} = \boldsymbol{\Omega}^*$ . Initially,

$$\left. \begin{aligned} \mathbf{U}^* &= \boldsymbol{\Omega}^* = 0 \\ \boldsymbol{\omega}^* &= \boldsymbol{\omega}_\infty^*(x, y, z, t) \\ \mathbf{u}^* &= \mathbf{u}_\infty^*(x, y, z, t) \end{aligned} \right\} \text{ for } t < 0. \tag{2.1}$$

The no-slip boundary conditions are that at the rigid surface  $y = y_s(x, z)$

$$\hat{\mathbf{u}} = 0 \text{ on } y = y_s(x, z), \quad -\infty < x, z < \infty \text{ for } t > 0. \tag{2.2}$$

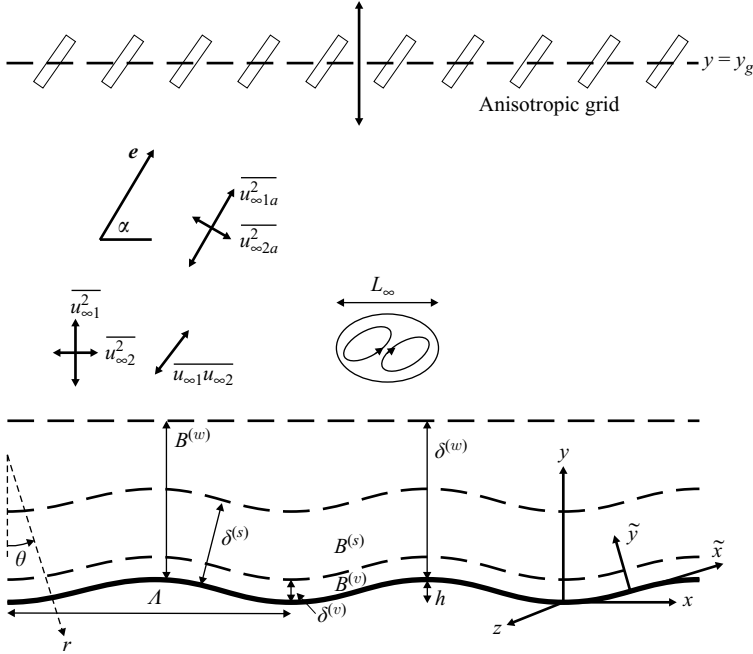


FIGURE 1. Definition sketch for anisotropic external turbulence (eccentrically orientated at an angle  $\alpha$  to the  $x$ -axis) near an undulating surface showing the grid, the rigid surface  $y_s(x)$  and the flow blocking regions: source region  $B^{(s)}$ , viscous region  $B^{(v)}$  and wave region for an undulating surface  $B^{(w)}$ . (In fact, we consider a flat surface for anisotropic external turbulence and an undulating surface for isotropic external turbulence.)

It is assumed that  $Re = v'_{\infty} L_{\infty} / \nu \gg 1$ , where  $v'_{\infty}$  is the r.m.s. value of  $u_{\infty}^*$ , and  $L_{\infty}$  is the integral length scale of  $u_{\infty}^*$ , and that the time for distortion (i.e. the time after the initial turbulence is distorted)  $T_D$  is small when compared with the Lagrangian time scale ( $T_L \sim L_{\infty} / v'_{\infty}$ ), so that

$$T_D / T_L \ll 1. \tag{2.3}$$

$T_L$  is both the decay time scale and the ‘turnover’ time (Tennekes & Lumley 1972) that nonlinear processes take to affect the anisotropy and spectra. In the absence of mean strain, Magnaudet (2003) has shown that these processes have a weak effect on the inhomogeneous distortion of large-scale structures near a boundary even when  $T_D / T_L \geq 1$ , as experiment indicates (e.g. Kit *et al.* 1997). When the mean strain grows, as it does in this case, nonlinear effects are significant when  $T_D \sim T_L$ .

The linearized governing equations for the fluctuating velocity are

$$\frac{\partial \mathbf{u}^*}{\partial t} = -\frac{\nabla p^*}{\rho} + \nu \nabla^2 \mathbf{u}^* + O\left(\frac{v_{\infty}^{\prime 2}}{L_{\infty}}\right), \tag{2.4a}$$

$$\frac{\partial \boldsymbol{\omega}^*}{\partial t} = \nu \nabla^2 \boldsymbol{\omega}^* + O\left(\frac{v_{\infty}^{\prime 2}}{L_{\infty}^2}\right). \tag{2.4b}$$

Note that, since the mean (ensemble-averaged) velocity  $\mathbf{U}^*$  and vorticity  $\boldsymbol{\Omega}^*$  are of order  $v'_{\infty}$  and  $v'_{\infty} / L_{\infty}$ , respectively, terms such as  $(\mathbf{U}^* \cdot \nabla) \mathbf{u}^*$  and  $(\boldsymbol{\Omega}^* \cdot \nabla) \mathbf{u}^*$  in (2.4a), (2.4b) are of order  $v_{\infty}^{\prime 2} / L_{\infty}$  and  $v_{\infty}^{\prime 2} / L_{\infty}^2$ . The mean velocity  $\mathbf{U}^*$  and mean vorticity

$\boldsymbol{\Omega}^* = \nabla \times \mathbf{U}^*$  generated by the distorted turbulence are given by

$$\frac{\partial \mathbf{U}^*}{\partial t} + (\mathbf{U}^* \cdot \nabla) \mathbf{U}^* = -\overline{(\mathbf{u}^* \cdot \nabla) \mathbf{u}^*} - \nabla P^* + \nu \nabla^2 \mathbf{U}^*, \quad (2.5a)$$

and

$$\frac{\partial \boldsymbol{\Omega}^*}{\partial t} = -\overline{(\mathbf{u}^* \cdot \nabla) \boldsymbol{\omega}^*} + \overline{(\boldsymbol{\omega}^* \cdot \nabla) \mathbf{u}^*} + \nu \nabla^2 \boldsymbol{\Omega}^*, \quad (2.5b)$$

where overbars denote time-averages. In two-dimensional flow where all inhomogeneities are in the  $(x, y)$ -plane (e.g. an undulating surface  $y = y_s(x)$ ), the initial growth of the mean vorticity is determined by

$$\frac{\partial \Omega_z^*}{\partial t} = \frac{\partial^2}{\partial x \partial y} (\overline{u^{*2}} - \overline{v^{*2}}) + \left( \frac{\partial^2}{\partial x^2} - \frac{\partial^2}{\partial y^2} \right) (-\overline{u^* v^*}) + \nu \nabla^2 \Omega_z^* + O\left(\frac{t^2 v_\infty^4}{L_\infty^4}\right). \quad (2.5c)$$

In the free stream above the surface

$$\left. \begin{aligned} \boldsymbol{\omega}^*(\mathbf{x}, t) &\rightarrow \boldsymbol{\omega}_\infty^*(\mathbf{x}, t) \\ \mathbf{u}^*(\mathbf{x}, t) &\rightarrow \mathbf{u}_\infty^*(\mathbf{x}, t) \end{aligned} \right\} \text{ as } y \rightarrow \infty. \quad (2.6a)$$

$\mathbf{u}_\infty^*, \boldsymbol{\omega}_\infty^*$  are assumed to be statistically homogeneous in the  $y$ - and  $z$ -directions, where for  $t < T_L$

$$\frac{d\boldsymbol{\omega}_\infty^*}{dt} = 0, \quad \frac{d\mathbf{u}_\infty^*}{dt} = 0. \quad (2.6b)$$

Since a non-zero mean flow field for  $t > 0$  exists only near the surface, the outer boundary conditions for the mean flow are

$$|\mathbf{U}^*|, \quad |\boldsymbol{\Omega}^*| \rightarrow 0 \quad \text{as } y \rightarrow \infty. \quad (2.7)$$

From (2.2), the boundary condition at the rigid surface is

$$\mathbf{U}^* = \mathbf{u}^* = 0. \quad (2.8)$$

Note that in previous studies of secondary flow the Reynolds stresses away from the boundary are driven by the mean shear. We consider here the general case where, away from the boundary, there is no mean shear and stresses are uniform. The blocking effects of the boundary induce gradients of the stresses and thence a growth of  $\partial \Omega_z^* / \partial t$  near the boundary.

## 2.2. The viscous, source and wave regions

Two separate regions with differing dynamics determine the distortion of the fluctuating velocity field. The outer, source region  $B^{(s)}$  has a thickness of the order of the integral scale  $L_\infty$ . The inner, viscous region  $B^{(v)}$  has thickness  $\delta^{(v)} \sim 4(t\nu)^{1/2}$ , which in the linear theory grows with time and within which the turbulent velocity decays to zero at the surface  $y = 0$ .

For the analysis of  $B^{(v)}$  we use the non-dimensional coordinates

$$\eta = y/(T_L \nu)^{1/2}, \quad X = x/L_\infty, \quad Z = z/L_\infty, \quad T = t\nu'_\infty/L_\infty, \quad (2.9)$$

and in  $B^{(s)}$  the definitions  $X, Z$  and  $T$  are unchanged while  $Y = y/L_\infty$ . Note that in the linear analysis ( $t < T_L$ ) the time scale for fluctuations in the viscous region is determined by the outer flow. The non-dimensional flow variables are

$$\omega_i = \omega_i^* L_\infty / \nu'_\infty, \quad u_i = u_i^* / \nu'_\infty, \quad p = p^* / (\rho \nu_\infty'^2), \quad (2.10)$$

which are conveniently expressed as sums of different terms associated with  $B^{(s)}$  and  $B^{(v)}$ :

$$\omega_i = \omega_{\text{oi}}(X, T) + \omega_i^{(s)}(X, T) + \omega_i^{(v)}(X, \eta, Z, T), \quad (2.11)$$

$$u_i = u_{\infty i}(\mathbf{X}, T) + u_i^{(s)}(\mathbf{X}, T) + u_i^{(v)}(X, \eta, Z, T). \quad (2.12)$$

In the source region, the vorticity remains the same as in the free stream, since there is no distortion to the mean flow (for  $t \leq T_L$ ). Hence the turbulent velocity is equal to the free-stream component plus an irrotational component  $-\nabla\Phi(\mathbf{X}, T)$ , i.e.

$$\mathbf{u} = \mathbf{u}_{\infty} - \nabla\Phi(\mathbf{X}, T), \quad (2.13)$$

and since  $\nabla \cdot \mathbf{u}^{(s)} = 0$ ,  $\Phi$  satisfies Laplace's equation

$$\nabla^2\Phi = 0. \quad (2.14)$$

The boundary conditions on  $\Phi$  are

$$\left. \begin{aligned} \partial\Phi/\partial Y &= u_{\infty 2}(X, Y=0, Z, T) \quad \text{on } Y=0, \quad t > 0, \\ \nabla\Phi &\rightarrow 0 \quad \text{as } Y \rightarrow \infty. \end{aligned} \right\} \quad (2.15)$$

The solution of (2.14) with (2.15) is

$$\Phi(X, Y, Z, T) = -\frac{1}{2\pi} \int_{-\infty}^{\infty} \int_{-\infty}^{\infty} \frac{u_{\infty 2}(X', Y'=0, Z', T)}{[(X-X')^2 + Y^2 + (Z-Z')^2]^{1/2}} dX' dZ'. \quad (2.16)$$

This solution is also valid in a spatially developing shear-free boundary layer, except within a distance of order  $L_{\infty}$  from  $X=0$ . The full solution with the upstream boundary condition is given by HG. Note that if the turbulence is to be analysed at a station  $X$  sufficiently far downstream of  $X=0$ , the upstream boundary condition becomes immaterial, and the solution is the same as for the time-developing solution considered here.

### 2.3. Fourier analysis of $B^{(s)}$ over a flat surface

The normalized turbulent velocity  $\mathbf{u}$  is expressed in terms of two- or three-dimensional Fourier transforms, which is equivalent to HG for stationary turbulence far above the surface. Near the surface, where the velocity is homogeneous in  $Z$  and  $X$ ,

$$\left\{ \begin{aligned} u_i(\mathbf{X}, T) \\ \Phi(\mathbf{X}, T) \end{aligned} \right\} = \int_{-\infty}^{\infty} \int_{-\infty}^{\infty} \left\{ \begin{aligned} \hat{u}_i \\ \hat{\Phi} \end{aligned} \right\} (K_1, K_3, Y, T) \exp\{i(K_1 X + K_3 Z)\} dK_1 dK_3. \quad (2.17)$$

In the free stream, where the turbulence is homogeneous in  $X, Y$  and  $Z$ ,

$$u_{\infty i}(\mathbf{X}, T) = \int_{-\infty}^{\infty} \int_{-\infty}^{\infty} \int_{-\infty}^{\infty} \mathcal{S}_{\infty i}(K_1, K_2, K_3, T) \exp\{i(\mathbf{K} \cdot \mathbf{X})\} dK_1 dK_2 dK_3. \quad (2.18)$$

$\mathbf{K}$  is a wavenumber normalized by  $L_{\infty}$ , so that  $K_1$  is effectively a non-dimensional frequency corresponding to an oscillation with frequency  $n$ .

In order to express the turbulence near the surface in terms of its spectrum in the free stream, we express  $\hat{u}_i$  and  $\hat{\Phi}$  in terms of  $\mathcal{S}_{\infty i}$  by the equations

$$\left\{ \begin{aligned} \hat{u}_i \\ \hat{\Phi} \end{aligned} \right\} (K_1, K_3; Y, T) = \int_{-\infty}^{\infty} \left\{ \begin{aligned} M_{il}(\mathbf{K}; Y) \\ \beta_l(\mathbf{K}; Y) \end{aligned} \right\} \mathcal{S}_{\infty i}(\mathbf{K}; T) dK_2, \quad (2.19)$$

where

$$M_{il} = M_{il}^{(\infty)} + M_{il}^{(s)}, \quad (2.20)$$

$$M_{il}^{(\infty)} = \delta_{ij} \exp\{i(K_2 Y)\}, \quad (2.21)$$

$$M_{il}^{(s)} = (-iK_1\beta_l, -\partial\beta_l/\partial Y, -iK_3\beta_l). \quad (2.22)$$

Substituting (2.18) and (2.19) into (2.16), we obtain

$$\beta_1 = \beta_3 = 0, \tag{2.23}$$

$$\beta_2 = -\frac{\exp\{-(K_1^2 + K_3^2)^{1/2} Y\}}{(K_1^2 + K_3^2)^{1/2}}, \tag{2.24}$$

$$M_{i1} = \delta_{i1} \exp\{iK_2 Y\}, \tag{2.25}$$

$$M_{i2} = \delta_{i2} \exp\{iK_2 Y\} + \left[ \frac{iK_1}{(K_1^2 + K_3^2)^{1/2}}, -1, \frac{iK_3}{(K_1^2 + K_3^2)^{1/2}} \right] \exp\{-(K_1^2 + K_3^2)^{1/2} Y\}, \tag{2.26}$$

$$M_{i3} = \delta_{i3} \exp\{iK_2 Y\}. \tag{2.27}$$

The three-dimensional Fourier transform  $\mathcal{S}_{\infty i}$  of a turbulent velocity component  $u_{\infty i}$  is related to the three-dimensional spectrum  $\Phi_{\infty ij}(\mathbf{K})$  by

$$\overline{\mathcal{S}_{\infty i}^+(K_1, K_2, K_3) \mathcal{S}_{\infty l}(K_1, K_2', K_3)} = \frac{\mathcal{X} \mathcal{Y}}{\pi^2} \delta(K_2 - K_2') \Phi_{\infty ij}(\mathbf{K}), \tag{2.28}$$

where + denotes a complex conjugate and  $L_{\infty \mathcal{X}}, L_{\infty \mathcal{Y}}$  and  $L_{\infty \mathcal{Z}}$  are the sides of the box within which the Fourier transforms of  $u_{\infty i}$  are defined. Equations (2.17) to (2.22) and (2.28) imply the normalized one-dimensional cross-spectrum for the velocities at one or two points  $\mathbf{X}_a, \mathbf{X}_b$  to be

$$\begin{aligned} \Theta_{ij}(\mathbf{X}_a, \mathbf{X}_b; K_1) &= \int_{-\infty}^{\infty} \int_{-\infty}^{\infty} M_{il}^+(\mathbf{K}; Y_a) M_{jm}(\mathbf{K}; Y_b) \\ &\quad \times \exp\{i(K_1(X_a - X_b) + K_3(Z_a - Z_b))\} \Phi_{\infty lm}(\mathbf{K}) dK_2 dK_3. \end{aligned} \tag{2.29}$$

The spectra  $\Theta_{ij}$  at one point are expressed as

$$\Theta_{11}(Y; K_1) = \Theta_{\infty 11}(K_1) + I_A(Y; K_1) + I_B(Y; K_1), \tag{2.30}$$

$$\begin{aligned} I_A(Y; K_1) &= iK_1 \int_{-\infty}^{\infty} \int_{-\infty}^{\infty} \frac{[\exp\{i(-K_2 Y)\} \Phi_{\infty 12} - \exp\{i(K_2 Y)\} \Phi_{\infty 21}]}{(K_1^2 + K_3^2)^{1/2}} \\ &\quad \times \exp\{-(K_1^2 + K_3^2)^{1/2} Y\} dK_2 dK_3, \end{aligned} \tag{2.31}$$

$$I_B(Y; K_1) = K_1^2 \int_{-\infty}^{\infty} \int_{-\infty}^{\infty} \frac{\exp\{-2(K_1^2 + K_3^2)^{1/2} Y\} \Phi_{\infty 22}}{K_1^2 + K_3^2} dK_2 dK_3, \tag{2.32}$$

$$\begin{aligned} \Theta_{22}(Y; K_1) &= \int_{-\infty}^{\infty} \int_{-\infty}^{\infty} [1 - 2 \cos(K_2 Y) \exp\{-(K_1^2 + K_3^2)^{1/2} Y\} \\ &\quad + \exp\{-2(K_1^2 + K_3^2)^{1/2} Y\}] \Phi_{\infty 22} dK_2 dK_3. \end{aligned} \tag{2.33}$$

Similar expressions for the  $\Theta_{33}$  and cross-spectra can also be derived. Note that  $\Theta_{11}$  is real because  $\Phi_{12}(\mathbf{K}) = \Phi_{21}^+(\mathbf{K})$  (Batchelor 1953).

#### 2.4. Three-dimensional energy spectrum for isotropic free-stream turbulence

In HG, the energy spectrum  $E(K)$  was assumed to have the typical ‘von Kármán’ form, corresponding to high- and moderate-Reynolds-number turbulence spectra (HRS); but the algebraic power law forms meant that analytic solutions for spectra and variances could not be derived. Here, we use the form of the ‘laboratory’ Reynolds-number spectrum (LRS) with exponential decay at high wavenumber (e.g. Townsend 1976),

$$E(K) = C_1 K^4 \exp\{-C_2 K^2\}, \tag{2.34}$$

where  $C_1 = 4/\pi^3$ ,  $C_2 = 1/\pi$  and the energy spectrum and wavenumber are normalized by  $v_\infty^2 L_\infty$  and  $L_\infty$ , respectively. We begin by considering isotropic free-stream turbulence so that  $E(K)$  is related to  $\Phi_{\infty ij}$  as (Batchelor 1953)

$$\Phi_{\infty ij}(\mathbf{K}) = \frac{E(K)}{4\pi K^4} (K^2 \delta_{ij} - K_i K_j). \quad (2.35)$$

### 2.5. Anisotropic free-stream turbulence

The three-dimensional spectrum tensor  $\Phi_{\infty ij}(\mathbf{K})$  for the axisymmetric free-stream turbulence depends only on  $\mathbf{K}$  and a unit vector,  $\mathbf{e}$ , in the direction of axial symmetry (Batchelor 1953). The most general second-order spectral tensor for such axisymmetric turbulence is of the form

$$\Phi_{\infty ij}(\mathbf{K}) = A_1 K_i K_j + A_2 e_i e_j + A_3 \delta_{ij} + A_4 e_i K_j + A_5 e_j K_i, \quad (2.36a)$$

in Cartesian-tensor notation, where  $A_1 \sim A_5$  are functions, not all independent, of  $\mathbf{K}$  and  $\mathbf{K} \cdot \mathbf{e}$ . Continuity of incompressible flow requires  $\Phi_{\infty ij}$  to be orthogonal to  $\mathbf{K}$ , i.e.  $\Phi_{\infty ij} K_j = 0$ , and symmetry in the indices  $i$  and  $j$  demands that  $A_4$  and  $A_5$  be equal. Hence, (2.36a) can be written as

$$\Phi_{\infty ij}(\mathbf{K}) = I_{ij} B_1(K, \mathbf{K} \cdot \mathbf{e}) + H_{ij} B_2(K, \mathbf{K} \cdot \mathbf{e}), \quad (2.36b)$$

where

$$I_{ij} = \delta_{ij} - \frac{K_i K_j}{K^2}, \quad (2.36c)$$

$$H_{ij} = e_i e_j + \frac{(\mathbf{K} \cdot \mathbf{e})^2}{K^2} \delta_{ij} - (\mathbf{K} \cdot \mathbf{e}) \frac{(e_i K_j + e_j K_i)}{K^2}, \quad (2.36d)$$

$$B_1(K, \mathbf{K} \cdot \mathbf{e}) = -K^2 A_1, \quad B_2(K, \mathbf{K} \cdot \mathbf{e}) = A_2. \quad (2.36e)$$

The interpretation of the ‘scalars’  $B_1$  and  $B_2$  and of (2.36) is much easier using the Craya–Herring frame (Craya 1958; Herring 1974), which is itself linked to the poloidal-toroidal decomposition in physical space (see the appendix in Cambon 2001 for details).

For isotropic turbulence

$$B_1(K, \mathbf{K} \cdot \mathbf{e}) = \frac{E(K)}{4\pi K^2}, \quad B_2(K, \mathbf{K} \cdot \mathbf{e}) = 0, \quad (2.37)$$

where  $E(K)$  is a three-dimensional energy spectrum.

Sreenivasan & Narashimha (1978) have considered various forms of axisymmetric turbulence in considering RDT and straining motions, such as two-dimensional contraction along a wind tunnel. They showed that if  $B_1$  and  $B_2$  are expanded in zonal harmonics with the Legendre polynomials  $P_{2m}(\cos \theta)$  as basis function, where  $\mathbf{K} \cdot \mathbf{e} = K \cos \theta$ ,

$$B_1(K, \theta) + B_2(K, \theta) = \sum_{m=0}^{\infty} F_{2m}(K) P_{2m}(\cos \theta), \quad (2.38a)$$

$$B_2(K, \theta) = \sum_{m=0}^{\infty} G_{2m}(K) P_{2m}(\cos \theta). \quad (2.38b)$$

The expansion in terms of spherical harmonics was generalized by Cambon & Teissèdre (1985) to arbitrary anisotropy. This expansion is consistent with that of Sreenivasan & Narasimha (1978) for axisymmetry, but not for that of Herring’s decomposition (1974).

Three ansatzes have been proposed. Ansatz 1 assumes that  $A_1$  and  $A_2$  depend only on  $K$ ; ansatz 2 assumes the same condition for  $A_2$  and  $A_3$  and similarly in ansatz 3 for  $A_1$  and  $A_3$ . Ansatz 1 represents what is possibly the simplest model for non-isotropic turbulence. It implies

$$F_{2m} = G_{2m} = 0 \quad \text{for } m = 1, 2, \dots$$

Hence from (2.36)–(2.38),

$$\Phi_{\infty ij}(\mathbf{K}) = I_{ij}(F_0(K) - G_0(K)) + H_{ij}G_0(K). \quad (2.39)$$

Ansatz 1 is adopted in our model, so

$$B_1 = B_1(K), \quad B_2 = B_2(K). \quad (2.40a)$$

The following forms of  $B_1$  and  $B_2$  are assumed in this study.

$$B_1 = C_1 K^2 \exp(-\lambda_1 K^2), \quad (2.40b)$$

$$B_2 = C_2 K^2 \exp(-\lambda_2 K^2), \quad (2.40c)$$

where  $C_1, C_2$  are constants and  $1/\lambda_1^{1/2}, 1/\lambda_2^{1/2}$  are proportional to the length scales of the isotropic and anisotropic components of this turbulent velocity field. For isotropic turbulence,  $C_2 = 0, C_1 = 1/\pi^4$  and  $\lambda_1 = 1/\pi$ . If the axis of symmetry has an angle  $\alpha$  to the surface, i.e.  $\mathbf{e} = (\cos \alpha, \sin \alpha, 0)$ , then the three-dimensional energy spectrum function becomes (in a frame of reference relative to a flat plate, at  $y = 0$ )

$$\Phi_{\infty 11} = (K_2^2 + K_3^2)C_1 \exp\{-\lambda_1 K^2\} + (K_2^2 + K_3^2 \cos^2 \alpha)C_2 \exp\{-\lambda_2 K^2\}, \quad (2.41a)$$

$$\Phi_{\infty 22} = (K_1^2 + K_3^2)C_1 \exp\{-\lambda_1 K^2\} + (K_1^2 + K_3^2 \sin^2 \alpha)C_2 \exp\{-\lambda_2 K^2\}, \quad (2.41b)$$

$$\begin{aligned} \Phi_{\infty 33} = & (K_1^2 + K_2^2)C_1 \exp\{-\lambda_1 K^2\} + (K_1^2 \cos^2 \alpha + K_1 K_2 \sin 2\alpha + K_2^2 \sin^2 \alpha) \\ & \times C_2 \exp\{-\lambda_2 K^2\}, \quad (2.41c) \end{aligned}$$

$$\begin{aligned} \Phi_{\infty 12} = \Phi_{\infty 21} = & -K_1 K_2 C_1 \exp\{-\lambda_1 K^2\} + \left(\frac{1}{2} K_3^2 \sin 2\alpha - K_1 K_2\right) \\ & \times C_2 \exp\{-\lambda_2 K^2\}, \quad (2.41d) \end{aligned}$$

$$\begin{aligned} \Phi_{\infty 23} = \Phi_{\infty 32} = & -K_2 K_3 C_1 \exp\{-\lambda_1 K^2\} - \left(\frac{1}{2} K_1 K_3 \sin 2\alpha + K_2 K_3 \sin^2 \alpha\right) \\ & \times C_2 \exp\{-\lambda_2 K^2\}, \quad (2.41e) \end{aligned}$$

$$\begin{aligned} \Phi_{\infty 31} = \Phi_{\infty 13} = & -K_1 K_3 C_1 \exp\{-\lambda_1 K^2\} - \left(K_1 K_3 \cos^2 \alpha + \frac{1}{2} K_2 K_3 \sin 2\alpha\right) \\ & \times C_2 \exp\{-\lambda_2 K^2\}. \quad (2.41f) \end{aligned}$$

Here,  $C_1, C_2, \lambda_1$  and  $\lambda_2$  are determined from the normalized variances, i.e. for each component

$$\int_{-\infty}^{\infty} \int_{-\infty}^{\infty} \int_{-\infty}^{\infty} \Phi_{\infty ii}(\mathbf{K}, \alpha = 0) \, d\mathbf{K} = \frac{\overline{u_{\infty ia}^2}}{\overline{u_{\infty 1a}^2}} = \left(1, \frac{1}{R}, \frac{1}{R}\right). \quad (2.42)$$

Since the spectra and wavenumbers are normalized in terms of the integral scale  $L_{\infty}$ ,

$$\Theta_{\infty 11}(K_1 \rightarrow 0, \alpha = 0)_{\text{aniso}} = \Theta_{\infty 11}(K_1 \rightarrow 0)_{\text{iso}} = \frac{1}{\pi}, \quad (2.43a)$$

	$R = 3/2$	$R = 2$
$\beta = 4$	$36/25\pi$	$1/\pi$
$\beta = 9$	$81/49\pi$	$1/\pi$

TABLE 1. Typical values of  $\lambda_2$  for given  $\beta$  and  $R$ .

and thence the coefficients are given by

$$\lambda_1 = \frac{1}{\pi} \text{Fn}(R, \beta)^{-2}, \tag{2.43b}$$

$$\lambda_2 = \frac{\beta}{\pi} \text{Fn}(R, \beta)^{-2}, \tag{2.43c}$$

$$C_1 = \frac{1}{\pi^4} \left(-1 + \frac{2}{R}\right) \text{Fn}(R, \beta)^{-5}, \tag{2.43d}$$

$$C_2 = \frac{2\beta^{5/2}}{\pi^4} \left(1 - \frac{1}{R}\right) \text{Fn}(R, \beta)^{-5}, \tag{2.43e}$$

where the function  $\text{Fn}(R, \beta)$  is

$$\text{Fn}(R, \beta) = \left(-1 + \frac{2}{R}\right) + 2\beta^{1/2} \left(1 - \frac{1}{R}\right). \tag{2.43f}$$

$R$  is the ratio of the variances of the free-stream turbulence components parallel and perpendicular to the principal axis (denoted by  $\overline{u_{\infty ia}^2}$ ),

$$R = \frac{\overline{u_{\infty 1a}^2}}{\overline{u_{\infty 2a}^2}} = \frac{\overline{u_{\infty 1a}^2}}{\overline{u_{\infty 3a}^2}}, \tag{2.43g}$$

and  $\beta$  is the ratio of the length scale of the isotropic and anisotropic components  $\lambda_1$  and  $\lambda_2$ , i.e.  $\beta = \lambda_2/\lambda_1$ . Note that

$$v_{\infty}^{\prime 2} = \frac{1}{3} \sum \overline{u_{\infty i}^2} = \overline{u_{\infty 1a}^2} \left(\frac{1 + 2/R}{3}\right). \tag{2.43h}$$

Here,  $R$  is restricted to lie within the range  $0 < R \leq 2$  in order to satisfy the non-negative Hermitian form of  $\Phi_{\infty ij}$ . (This also corresponds approximately to the range of anisotropy for which axisymmetric turbulence can persist over several integral time scales ( $T_L$ ), e.g. disperse vortex rings.) When  $R = 1$ , the turbulence is isotropic. Table 1 shows typical values of  $\lambda_2$  for given  $\beta$  and  $R$ .

Figure 2 shows the one-dimensional power spectra  $\Theta_{\infty ij}$  for  $R = 2$  and  $\beta = 4$ . These are obtained by integrating three-dimensional energy spectrum functions  $\Phi_{\infty ij}$  with respect to  $K_2$  and  $K_3$ . Here we note that in the model spectra, the anisotropy is significant at large scales, while the small scales remain isotropic (i.e.  $\beta \gg 1$ ), a characteristic of the spectrum of most high-Reynolds-number anisotropic turbulence (e.g. Kaimal *et al.* 1972). Figure 3 shows the one-dimensional power spectra  $\Theta_{\infty 12}$  for  $R = 3/2, 2$  and  $\beta = 4$ . The larger anisotropy (the larger  $R$ ) induces larger Reynolds stress in the free stream. The Reynolds stress takes its maximum when  $\alpha = \pi/4$ .

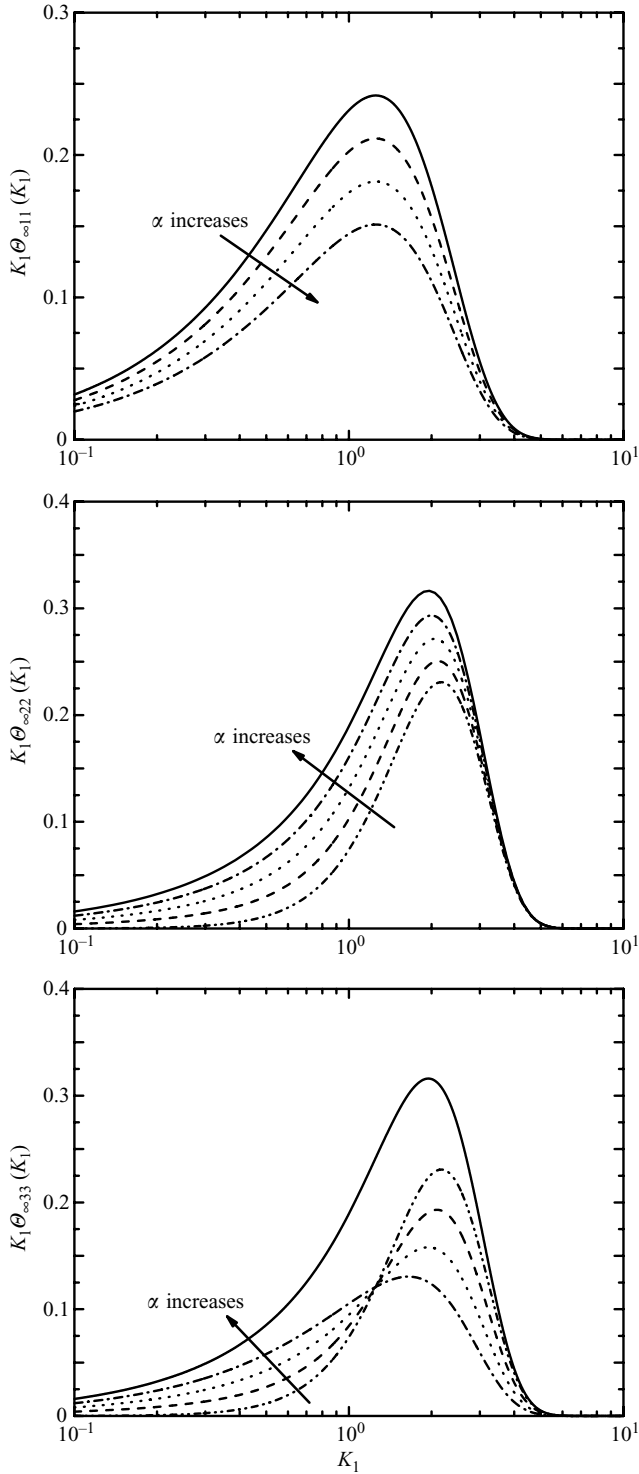


FIGURE 2. The one-dimensional power spectra  $K_1\Theta_{\infty ii}$  for homogeneous anisotropic (axisymmetric) free-stream turbulence for  $R=2$  and  $\beta=4$ . —, isotropic ( $R=1$ ); — · — · — · — · —,  $\alpha=0$ ; - - -,  $\alpha=\pi/6$ ; - · - ·,  $\alpha=\pi/4$ ; · · · ·,  $\alpha=\pi/3$ .  $K_1\Theta_{\infty 11}$  for  $\alpha=0$  is identical to that for the isotropic case (—).

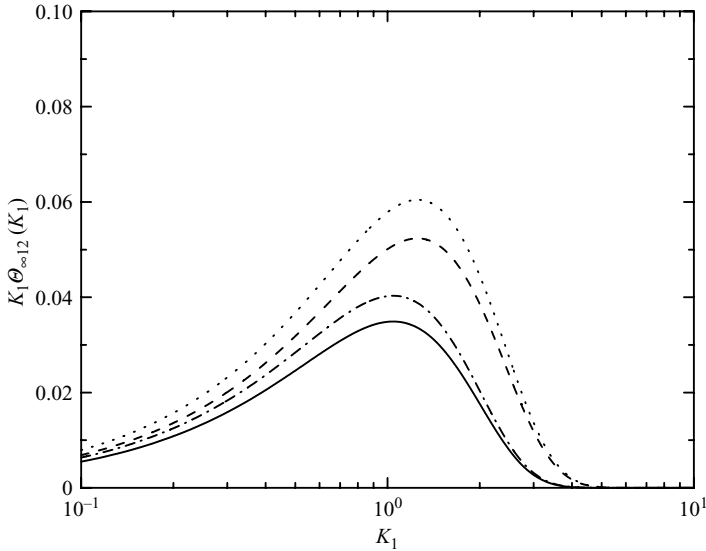


FIGURE 3. The one-dimensional power spectra  $\Theta_{\infty 12}$  for homogeneous axisymmetric free-stream turbulence for  $R = 3/2, 2$  and  $\beta = 4$ . —,  $R = 3/2, \alpha = \pi/6, \pi/3$ ; - - -,  $R = 3/2, \alpha = \pi/4$ ; - · - ·,  $R = 2, \alpha = \pi/6, \pi/3$ ; · · ·,  $R = 2, \alpha = \pi/4$ . Note  $\Theta_{\infty 12} = 0$  for isotropic free-stream turbulence and for  $\alpha = 0$  in anisotropic turbulence.

### 3. Turbulence near a flat plate of arbitrary orientation

#### 3.1. Effects of spectral form on isotropic shear-free boundary layer on a flat plate

##### 3.1.1. Turbulence intensities

For the ‘laboratory’ Reynolds-number spectrum (LRS), analytical solutions of the variances for isotropic free-stream turbulence ( $R = 1$ ) are given by

$$\begin{aligned} \overline{u_1^2/u_{\infty 1}^2} = \overline{u_3^2/u_{\infty 3}^2} = \frac{1}{2}(\pi Y^2 + 3) + \frac{\pi Y^2}{4} \exp\left\{-\frac{\pi Y^2}{4}\right\} - \frac{\pi Y}{8}(\pi Y^2 + 2) \operatorname{erfc}\left\{\frac{\pi^{1/2} Y}{2}\right\} \\ - \frac{\pi Y}{4}(2\pi Y^2 + 3) \exp\{\pi Y^2\} \operatorname{erfc}\{\pi^{1/2} Y\}, \quad (3.1) \end{aligned}$$

$$\begin{aligned} \overline{u_2^2/u_{\infty 2}^2} = 2 + \pi Y^2 - 2 \exp\left\{-\frac{\pi Y^2}{4}\right\} \left(\frac{\pi Y^2}{4} + 1\right) + \frac{\pi Y}{4}(\pi Y^2 + 6) \operatorname{erfc}\left\{\frac{\pi^{1/2} Y}{2}\right\} \\ - \frac{\pi Y}{2}(2\pi Y^2 + 3) \exp\{\pi Y^2\} \operatorname{erfc}\{\pi^{1/2} Y\}. \quad (3.2) \end{aligned}$$

Figures 4 and 5 show the turbulence intensities, normalized by the turbulence intensities  $\overline{u_{\infty i}^2}$  in the free stream. Here the turbulence intensity in the spanwise direction  $\overline{u_3^2}$  is identical to that in the streamwise direction  $\overline{u_1^2}$ . In  $B^{(s)}$  the normal component  $\overline{u_2^2}$  decreases, while the streamwise and spanwise component,  $\overline{u_1^2}$  and  $\overline{u_3^2}$ , increase towards the surface in such a way that the turbulence kinetic energy is restored at the surface ( $Y = 0$ ) to the value in the free stream. The blocking effects by the surface with LRS are relatively greater than with HRS. The vertical velocity fluctuations decrease and streamwise and spanwise velocity fluctuations increase faster in the vicinity of the surface compared to the high-Reynolds-number case. Then, as HG found,  $\overline{u_1^2}$  and  $\overline{u_3^2}$  first decrease to values below  $\overline{u_{\infty 1}^2}$  and  $\overline{u_{\infty 3}^2}$  before increasing to

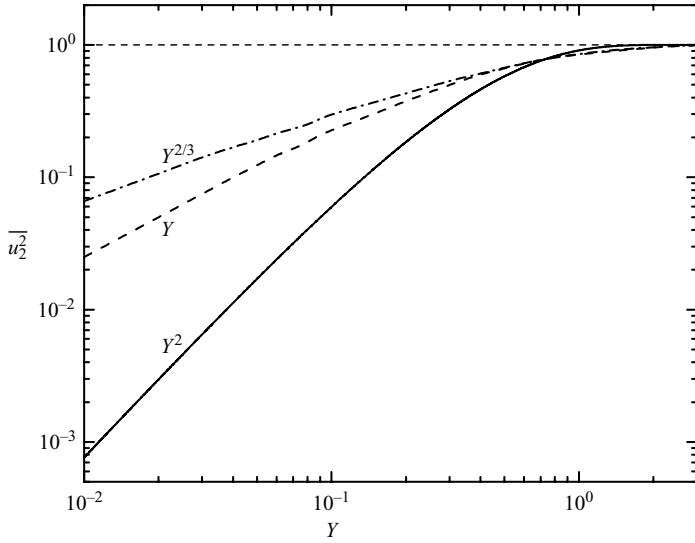


FIGURE 4. Turbulence intensities of the normal velocity fluctuations in the source layer. —, exponential spectrum in present study (LRS); - - -, HG for ‘high Reynolds numbers’ (von Kármán spectra); - · - ·, HG for ‘moderate Reynolds numbers’ (Townsend spectrum). Note the different slopes as  $y \rightarrow 0$ .

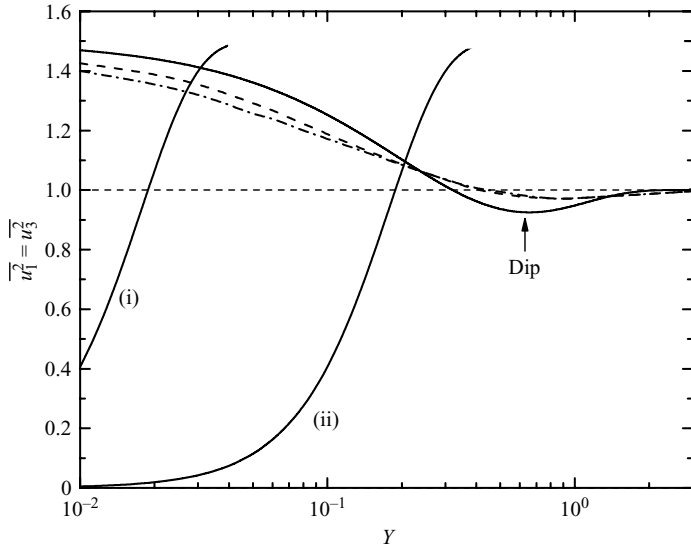


FIGURE 5. Turbulence intensities of the streamwise and spanwise velocity fluctuations in the viscous region  $B^{(v)}$  and the source region  $B^{(s)}$ . In  $B^{(s)}$ : symbols as in figure 4. In  $B^{(s)}$ : (i) non-dimensional time  $t\nu/L_\infty^2 = 10^{-4}$ ; (ii)  $t\nu/L_\infty^2 = 10^{-2}$ . Note the greater dip with LRS and the increase of  $\overline{u_1^2}$  toward the surface at  $y=0$  extends farther from the surface.

their asymptotic values. As a result of stronger blocking this ‘dip’ is greater with the LRS. A similar dip in the turbulence kinetic energy is found with the LRS: the lowest value is 0.784, while they are 0.865 at high Reynolds numbers and 0.845 at moderate Reynolds numbers. The decrease in  $\overline{u_2^2}$  is associated with a rise in the mean pressure.

Asymptotic expressions for  $\overline{u_1^2}(=\overline{u_3^2})$  and  $\overline{u_2^2}$  can be obtained near the surface (when  $\delta^{(v)} \rightarrow 0$ ). As  $Y \rightarrow 0$ ,

$$\overline{u_1^2}/\overline{u_{\infty 1}^2} = \overline{u_3^2}/\overline{u_{\infty 3}^2} = \frac{3}{2} - \pi Y + \frac{5}{2}\pi Y^2 + O(Y^3), \quad (3.3)$$

$$\overline{u_2^2}/\overline{u_{\infty 2}^2} = \frac{5}{2}\pi Y^2 + O(Y^3). \quad (3.4)$$

Note that with LRS the derivative of  $\overline{u_2^2}$  at the surface is zero whereas the derivatives of  $\overline{u_1^2}$  at the surface with high Reynolds spectra (HRS) have non-zero values. Asymptotic expressions for  $\overline{u_1^2}(=\overline{u_3^2})$  and  $\overline{u_2^2}$  for  $Y \rightarrow \infty$  are also obtained:

$$\overline{u_1^2}/\overline{u_{\infty 1}^2} = \overline{u_3^2}/\overline{u_{\infty 3}^2} = 1 + \frac{3}{8\pi Y^2} + \frac{1}{\pi Y^2} \exp\left\{-\frac{\pi Y^2}{4}\right\}, \quad (3.5)$$

$$\overline{u_2^2}/\overline{u_{\infty 2}^2} = 1 + \frac{3}{4\pi Y^2} - \frac{6}{\pi Y^2} \exp\left\{-\frac{\pi Y^2}{4}\right\}. \quad (3.6)$$

### 3.1.2. Integral length scales near the surface

The integral length scales near the surface are obtained from the variances and spectra.

$${}^x L_{11} = \frac{L_{\infty}}{\overline{u_1^2}(Y \rightarrow 0)/\overline{u_{\infty 1}^2}} = \frac{2L_{\infty}}{3 - 2\pi Y}, \quad (3.7)$$

$${}^x L_{22} = \frac{\pi\Theta_{22}(K_1 = 0)}{\overline{u_2^2}(Y \rightarrow 0)/\overline{u_{\infty 2}^2}} = \frac{4 - 10Y}{10 - 9\pi Y} L_{\infty}. \quad (3.8a)$$

Therefore, for isotropic turbulence,  ${}^x L_{11}(Y \rightarrow 0) = {}^x L_{33}(Y \rightarrow 0) = 2L_{\infty}/3$  (which is independent of the form of the spectrum), but  ${}^x L_{22}(Y \rightarrow 0) = 2L_{\infty}/5$ . By comparison with high Reynolds number turbulence, when there is a larger distortion of the spectra (Carloti 2001),

$${}^x L_{22} \propto Y; \quad \text{as } Y \rightarrow 0. \quad (3.8b)$$

The latter (HG) result is generally assumed in turbulence models for high-Reynolds-number turbulence.

### 3.1.3. Comparison with previous measurement

The variance at ‘laboratory’ Reynolds numbers are compared with the previous mixing-box experiment at low Reynolds number of  $Re_L = 40$  (McDougall 1979). It is found that the present study underpredicts the decrease in  $\overline{u_2^2}$ . In this experiment (and also Uzkan & Reynolds 1967), no amplification of the horizontal velocity component was found because the thickness of the viscous surface layer was comparable to that of the source layer. In the experiment by McDougall, the thickness of the viscous layer is estimated as  $\delta^{(v)}/L_{\infty} \sim 0.2$  and the solution of  $\overline{u_1^2}$  in  $\delta^{(v)}$  is plotted in figure 6. The profile of  $\overline{u_1^2}$  in  $\delta^{(v)}$  explains why the data of McDougall show no amplification near the surface. Note that in the experiment with higher-Reynolds-number turbulence (e.g. Thomas & Hancock 1977; Brumley & Jirka 1987; Hannoun, Fernando & List 1988; Kit *et al.* 1997) significant amplification of  $\overline{u_1^2}$  was found.

## 3.2. Impingement of anisotropic turbulence onto a flat surface and mean flow generation

Here we consider homogeneous axisymmetric free-stream turbulence. The axis of symmetry lies at an angle  $\alpha$  to the surface so that  $\mathbf{e} = (\cos \alpha, \sin \alpha, 0)$ . The analytical

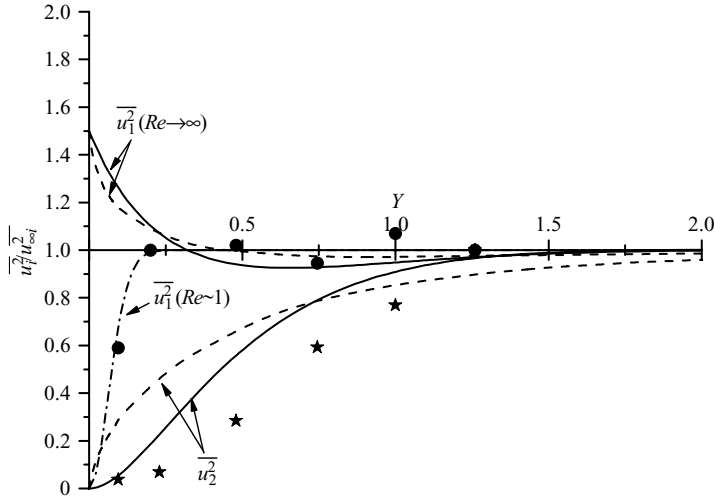


FIGURE 6. Vertical distributions of turbulence intensities. —, present study (in  $B^{(s)}$ ); ---, HG at high Reynolds numbers (in  $B^{(s)}$ ); ● and ★,  $\overline{u_1^2}$  and  $\overline{u_2^2}$  in mixing-box turbulence at  $Re_L = 40$  (McDougall 1979); - · -, Estimated  $\overline{u_1^2}$  ( $= \overline{u_3^2}$ ) in  $B^{(v)}$  corresponds to McDougall's experiment.

solutions of the variances and covariance for this axisymmetric free-stream turbulence are given in the Appendix. All these profiles near the surface are independent of  $\beta$ . The variances in the free stream as  $Y \rightarrow \infty$  are

$$\overline{u_1^2} / \overline{u_{\infty 1a}^2} = 1 - \sin^2 \alpha \left( 1 - \frac{1}{R} \right), \tag{3.9a}$$

$$\overline{u_2^2} / \overline{u_{\infty 1a}^2} = \frac{1}{R} + \sin^2 \alpha \left( 1 - \frac{1}{R} \right), \tag{3.9b}$$

$$\overline{u_3^2} / \overline{u_{\infty 1a}^2} = \frac{1}{R}, \tag{3.9c}$$

$$\overline{u_1 u_2} / \overline{u_{\infty 1a}^2} = \frac{1}{2} \sin 2\alpha \left( 1 - \frac{1}{R} \right), \tag{3.9d}$$

where  $\overline{u_{\infty 1a}^2}$  is the variance in the direction parallel to  $e$ . Note that  $\overline{u_{\infty 1a}^2} = \overline{u_{\infty 1}^2}$  when  $\alpha = 0$ . Note that the sign of  $\overline{u_1 u_2}$  is essentially determined by whether the turbulence along the axis of symmetry is greater or less than in the plane perpendicular to the axis, i.e.  $\overline{u_1 u_2} > 0$  if  $R > 1$ ,  $\overline{u_1 u_2} < 0$  if  $R < 1$ .

3.2.1. The case of  $\alpha = 0$  when the axis of symmetry lies parallel to the surface

Streamwise and spanwise turbulence intensities are amplified whereas the vertical intensity decreases toward the surface as for isotropic free-stream turbulence. However, the relative amplification of  $\overline{u_1^2}$ ,  $\overline{u_3^2}$  varies depending on  $R$ . From (A 1)–(A 3) we have as  $Y \rightarrow 0$

$$\overline{u_1^2} / \overline{u_{\infty 1}^2} = \frac{5}{4} + \frac{1}{4R}, \tag{3.10a}$$

$$\overline{u_2^2} / \overline{u_{\infty 1}^2} = 0, \tag{3.10b}$$

$$\overline{u_3^2} / \overline{u_{\infty 1}^2} = -\frac{1}{4} + \frac{7}{4R}, \tag{3.10c}$$

which satisfies the general condition (HG) that

$$\begin{aligned} \sum_{i=1}^3 \overline{u_i^2}(Y \rightarrow 0) &= \sum_{i=1}^3 \overline{u_{\infty i}^2} = \left(1 + \frac{2}{R}\right) \overline{u_{\infty 1a}^2} \\ &= \left(1 + \frac{2}{R}\right) \overline{u_{\infty 1}^2} \quad \text{for the case } \alpha = 0. \end{aligned} \tag{3.11}$$

In this type of homogeneous axisymmetric free-stream turbulence,  $\overline{u_2^2}$  is damped by the wall, but the normal velocity is not distributed equally in the  $X$ - and  $Z$ -directions as  $Y \rightarrow 0$ . Reynolds shear stresses are zero as for the isotropic case when  $\alpha = 0$ . Note that the dependence on  $R$  in these results (3.10a), (3.10c) were obtained using a particular spectrum. However, this sensitivity is small, since varying  $\beta (= \lambda_2/\lambda_1)$  has no effect on variances at the surface and only a small effect when  $Y \sim 1$ . For example, it only changes  $\overline{u_2^2}/\overline{u_{\infty 1}^2}$  by 10% as  $\beta$  varies from  $\beta = 4$  to  $\beta = 9$  for  $R = 3/2$ . In figure 7, the variances are normalized by their values in the free stream,  $\overline{u_{\infty i}^2}$ . It is found that the blocking effects become less significant for anisotropic free-stream turbulence if the axis of symmetry lies parallel to the surface. Note that these formula are only valid for  $0 < R < 2$ .

3.2.2. The case of  $\alpha \neq 0$  when the axis of symmetry lies at an angle to the surface

$\overline{u_1^2}$  decreases and  $\overline{u_3^2}$  increases near the surface with increasing  $\alpha$  when the turbulence intensities are normalized by  $\overline{u_{\infty 1a}^2}$  which is the component parallel to the axis of symmetry (see figure 1). From (A 1)  $\sim$  (A 5) we have as  $Y \rightarrow 0$

$$\overline{u_1^2}/\overline{u_{\infty 1a}^2} = \frac{5}{4} + \frac{1}{4R} - \frac{3}{4} \sin^2 \alpha \left(1 - \frac{1}{R}\right), \tag{3.12a}$$

$$\overline{u_2^2}/\overline{u_{\infty 1a}^2} = 0, \tag{3.12b}$$

$$\overline{u_3^2}/\overline{u_{\infty 1a}^2} = -\frac{1}{4} + \frac{7}{4R} + \frac{3}{4} \sin^2 \alpha \left(1 - \frac{1}{R}\right). \tag{3.12c}$$

In the limit  $R \rightarrow 0$ ,  $\overline{u_{\infty 1}^2}/\overline{u_{\infty 2}^2} \rightarrow 0$ , and  $\overline{u_{\infty 2}^2} = \overline{u_{\infty 3}^2}$ . However, because  $\beta$  is finite, the flow field varies in three directions. This is why, as  $Y \rightarrow 0$ ,  $\overline{u_1^2}/\overline{u_{\infty 2}^2} \rightarrow 1/4$ , while  $\overline{u_3^2}/\overline{u_{\infty 2}^2} \rightarrow 7/4$ . In two-dimensional turbulence where  $\overline{u_{\infty 1}^2} = 0$  and  $\partial/\partial x = 0$ ,  $\overline{u_3^2}/\overline{u_{\infty 2}^2} \rightarrow 2$  as  $Y \rightarrow 0$ .

Figure 8 shows the vertical distributions of the Reynolds stress, normalized by the Reynolds stress in the free stream,  $\overline{u_1 u_2}(Y \rightarrow \infty)$  (in the frame parallel to the surface). Note that  $\overline{u_1 u_2}$  varies with  $R$  and  $\beta$ , but not  $\alpha$ . By contrast, the profiles of  $\overline{u_1^2}$  and  $\overline{u_3^2}$  do depend on  $\alpha$ . The normalized Reynolds stress near the surface where it tends to zero is independent of  $R$  as well as  $\alpha$ , and is given by

$$\overline{u_1 u_2}(Y)/\overline{u_1 u_2}(Y \rightarrow \infty) = \frac{3}{4} \left\{ \left(\frac{\pi}{\lambda_2}\right)^{1/2} Y - \frac{1}{\lambda_2} Y^2 \right\} \quad \text{as } Y \rightarrow 0. \tag{3.13}$$

Thus,  $\overline{u_1 u_2}$  near the surface is determined by  $Y/\lambda_2^{1/2}$ , i.e. the ratio of the normal coordinate and the length scale of the additional anisotropic component of the turbulence (defined in (2.40)).

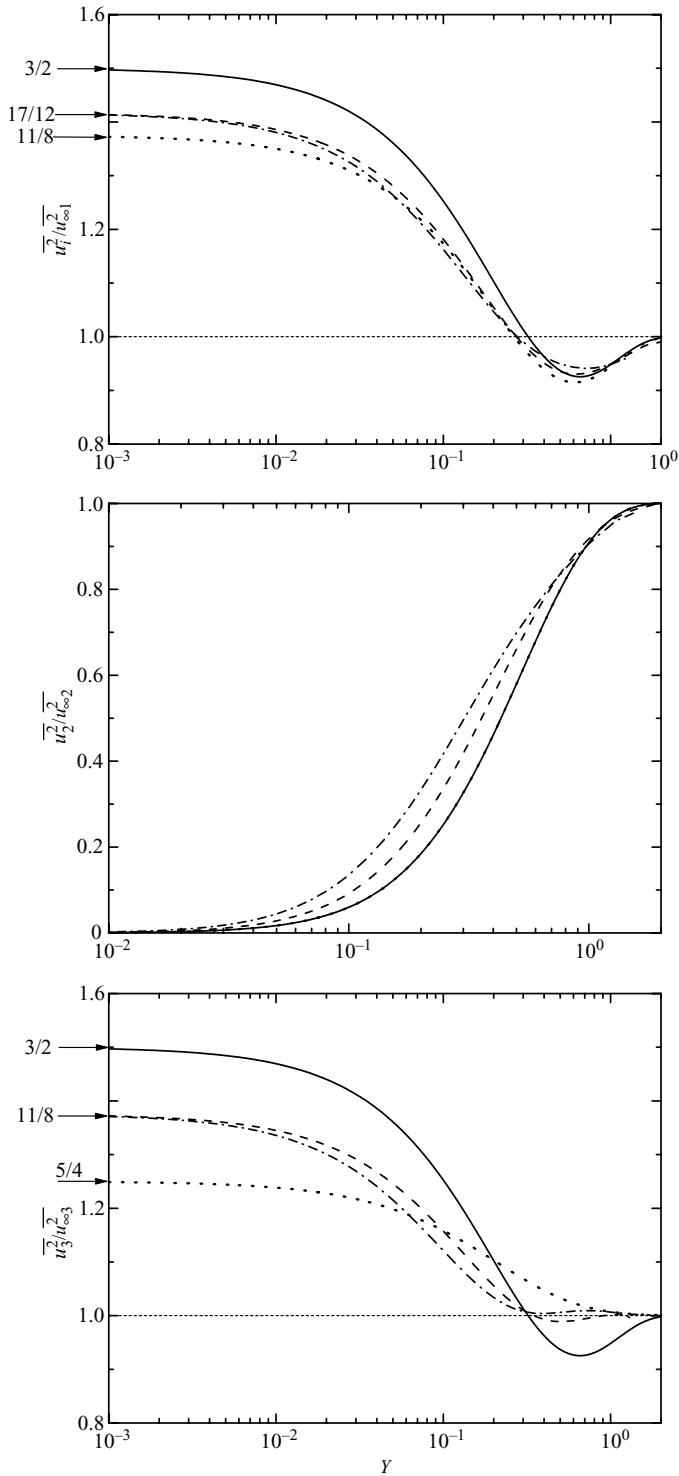


FIGURE 7. The three components of anisotropic turbulence near a flat wall normalised by their free-stream value (using coordinates parallel and normal to the surface). —, isotropic case ( $R = 1$ ); ---,  $R = 3/2$ ,  $\beta = 4$ ; - · - ·,  $R = 3/2$ ,  $\beta = 9$ ; · · · ·,  $R = 2$ ,  $\beta = 4$ .

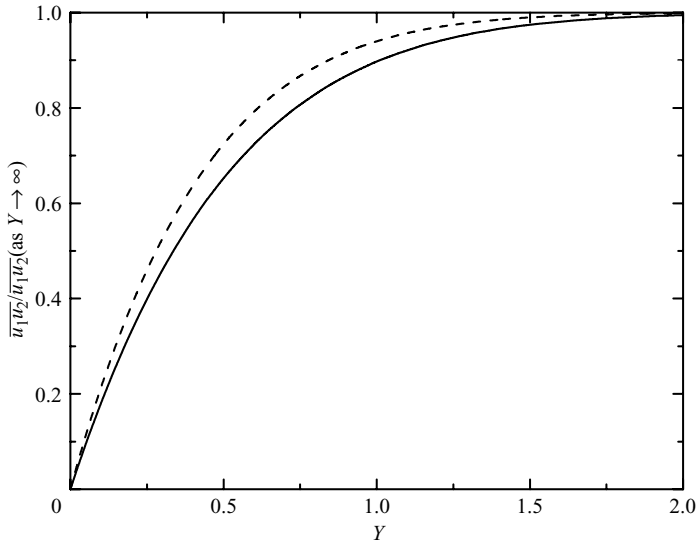


FIGURE 8. Vertical distributions of the Reynolds stress normalized by the value in the free stream for  $\beta = \lambda_2/\lambda_1 = 4$ . —,  $R = 3/2$ ,  $\alpha = \pi/6, \pi/4, \pi/3$ ; ---,  $R = 2$ ,  $\alpha = \pi/6, \pi/4, \pi/3$ . Note that this normalized profile is independent of  $\alpha$ .

3.3. Secondary motions near plane boundaries

In this section, we analyse how secondary motions can be generated near a plane boundary. It follows, by integrating the normalized form of (2.5a), that the time-averaged equation for streamwise secondary flow near the surface is given by

$$\frac{\partial U}{\partial t} = - \frac{\partial}{\partial y} \overline{u_1 u_2}. \tag{3.14}$$

Substituting (3.12) into (3.14) and referring to (2.43h), we have (in dimensional terms) for  $t \ll T_L$

$$U^* \sim \frac{3t}{8} \sin 2\alpha \left(1 - \frac{1}{R}\right) \left(\frac{3}{1 + 2/R}\right) \left\{ \frac{2v_\infty'^2}{\lambda_2 L_\infty^2} y - \frac{v_\infty'^2}{L_\infty} \left(\frac{\pi}{\lambda_2}\right)^{1/2} \right\} \text{ for } y \ll L_\infty. \tag{3.15}$$

Thus, horizontal secondary flow exists near a flat rigid surface provided the axis of the anisotropic (e.g. axisymmetric) turbulence in the free stream does not lie on a plane which is perpendicular or parallel to the surface. For small  $t$ , the secondary flow grows near the surface linearly with time and decreases with distance  $y$  above the surface. Here we are ignoring viscous stresses in the viscous layer where  $U \rightarrow 0$  at  $Y = 0$ . Even for anisotropic high-Reynolds-number turbulence (e.g. in a shear flow where  $\Theta_{12}(K_1) \propto K_1^{-7/3}$ , Mann 1994) the same effect as described in (3.15) would occur (Wong 1985). Note that the direction of  $U$  is opposite to the projection of  $e$  onto the plane (for  $R > 1$ ) (i.e.  $U/|U| = ((e \wedge n) \wedge n)(1 - 1/R)$ ), where  $n$  is a unit vector normal to the surface. Equation (3.15) is finite as  $R \rightarrow 0$ , and the sign of  $U$  changes as  $R$  decreases below 1.0.

As with other secondary flows driven by normal stresses, nonlinear effects develop and the mean velocity reaches a quasi-steady state when  $t \sim T_L \sim L_\infty/u'_{\infty s}$ , where  $u'_{\infty s}$  is the r.m.s. velocity associated with the mean shear. Then, the mean shear in the source layer induces Reynolds stress gradients ( $\sim U^* u'_{\infty s}/L_\infty$ ) with opposite sign to those produced by the blocking of the anisotropic external turbulence (i.e. given by

(3.13)). So that, an order of magnitude estimate for the resulting mean velocity  $U^*$  is

$$U^*(t \sim T_L) \sim \sin 2\alpha \left(1 - \frac{1}{R}\right) v'_{\infty} \left(\frac{v'_{\infty}}{u'_{\infty s}}\right). \quad (3.16)$$

Since in most shear flows near a rigid surface,  $u'_{\infty s} \sim U^*/10$  (depending on the roughness of the surface and the Reynolds number of the flow, e.g. Townsend 1976), we estimate that

$$U^* \sim \left\{ \sin 2\alpha \left(1 - \frac{1}{R}\right) \right\}^{1/2} v'_{\infty}. \quad (3.17)$$

A full nonlinear analysis or numerical simulation is required to study these flow mechanisms.

#### 4. Turbulence and mean flow over an undulating surface

##### 4.1. Distortion of the turbulence

Now consider a rigid undulating surface of low slope, amplitude  $h$  and long wavelength  $\Lambda$ , defined by

$$y_s(x) = h(1 - \cos(2\pi x/\Lambda)), \quad (4.1)$$

or in non-dimensional terms (based on the length scale  $L_{\infty}$ ),

$$Y_s(X) = H(1 - \cos kX), \quad (4.2)$$

where  $H = h/L_{\infty} \ll 1$ ,  $k = 2\pi L_{\infty}/\Lambda \ll 1$ . The surface is introduced at  $t=0$  into an isotropic turbulent velocity field  $\mathbf{u}_{\infty}(\mathbf{x}, t)$ . It is assumed that the turbulence above the surface wave (where  $y \geq L_{\infty}$ ) is homogeneous and approximately isotropic. The turbulent flow is not periodic. Its integral scale is less than the wavelength of the surface. The calculation shows how a mean flow is set up by the undulating surface. This implies that the mean flow has a larger wavelength than that of the turbulence, which is quite usual in distorted turbulent flows. (In the first problem the wavelength of the mean flow is effectively infinite.) As with turbulence over the flat plate initially there is no mean flow to distort the turbulent vorticity. Therefore outside the viscous layer  $B^{(v)}$ , the perturbations to the turbulence are determined by the blocking effects of (2.13) and (2.14), namely,

$$\nabla\Phi \cdot \mathbf{n} = \mathbf{u}_{\infty} \cdot \mathbf{n} \quad \text{on } Y = Y_s(X). \quad (4.3)$$

Here

$$\mathbf{n} = (-Hk \sin kX, 1, 0)/(1 + H^2k^2 \sin^2 kX), \quad (4.4a)$$

$$\mathbf{n} \simeq \left(\frac{-X}{R_c}, 1, 0\right) \quad \text{when } |kX| \ll 1, \quad (4.4b)$$

where  $R_c$  is the normalized radius of curvature  $R_c = 1/(Hk^2)$ . Then the boundary condition for the source layer transfer function  $M_{il}^{(s)}$  in (2.22) on  $y = y_s(X)$  is

$$M_{il}^{(s)} \cdot n_i = \frac{(-M_{1l}^{\infty} Hk \sin kX + M_{2l}^{\infty}) \exp\{i(K_1 X + K_2 H(1 - \cos kX) + K_3 Z)\}}{(1 + H^2k^2 \sin^2 kX)}. \quad (4.5)$$

The solution to (4.3) using a formal solution in terms of  $Hk$  and  $K/k$  has been obtained by Wong (1985). The results are even more complex than those obtained in §3.

It is more instructive to consider the simple problem of a sinusoidal velocity field (i.e. a single Fourier component of the turbulence in (2.17)),

$$u_{\infty i} = \mathcal{S}_{\infty i} \exp\{i(K_j X_j)\}, \tag{4.6}$$

as it impacts onto a circular (or a parabolic) surface (which is the trough or peak of the surface (4.1))

$$Y_s = \pm Hk^2 X^2/2 = X^2/(2R_c^2), \tag{4.7}$$

over a distance  $1 \gg |kX|$ , where  $1 \gg k$ . The non-dimensional radius of curvature is  $R_c = 1/(Hk^2)$ . Note that the radius of curvature is negative on the peak of the undulation. The solution to (4.3) can be obtained in polar coordinates  $(r, \theta)$  subject to the boundary condition

$$\begin{aligned} \frac{\partial \Phi}{\partial R} = & -\mathcal{S}_{\infty 1} \sin \theta \exp\{i(K_1 \tilde{X} \cos \theta + K_3 Z)\} \\ & + \mathcal{S}_{\infty 2} \cos \theta \exp\{i(K_1 \tilde{X} \cos \theta + K_3 Z)\} \quad \text{on } N = 0, \end{aligned} \tag{4.8}$$

where  $\tilde{X}$  and  $\tilde{Y}$  are the intrinsic coordinates along and normal to the surface, respectively. Note that  $\tilde{X} = \theta R_c$  and  $\tilde{Y} = R_c - R$ ;  $R = r/(Hk^2)$ .

Seeking a perturbation expansion in terms of  $1/(KR_c)$ , it follows that

$$\Phi = \left( \hat{\Phi}^{(0)}(\mathbf{K}, \tilde{Y}) + \frac{1}{KR_c} \hat{\Phi}^{(1)}(\mathbf{K}, \tilde{Y}) \cdots \right) \exp\{i(K_1 \tilde{X} + K_3 Z)\}, \tag{4.9a}$$

where (for the idealised fluctuation of (4.6))

$$K = [K_1^2 + K_2^2 + K_3^2]^{1/2} \sim 1, \tag{4.9b}$$

and

$$\left( \frac{\partial^2}{\partial \tilde{Y}^2} - K_{13}^2 \right) \hat{\Phi}^{(0)} = 0, \tag{4.9c}$$

subject to the boundary condition

$$\frac{\partial \hat{\Phi}^{(0)}}{\partial \tilde{Y}} = +\mathcal{S}_{\infty 2} \exp\{i(K_1 \tilde{X} + K_3 Z)\}. \tag{4.9d}$$

The solution of this problem may be expressed as

$$\hat{\Phi}^{(0)} = -\frac{\mathcal{S}_{\infty 2}}{K_{13}} \exp\{-K_{13} \tilde{Y}\}, \tag{4.10}$$

where  $K_{13} = \sqrt{K_1^2 + K_3^2}$ .

For the next order in the perturbation expansion, we must solve Laplace's equation in cylindrical coordinates,

$$\left( \frac{\partial^2}{\partial \tilde{Y}^2} - K_{13}^2 \right) \hat{\Phi}^{(1)} = -K \frac{\partial \hat{\Phi}^{(0)}}{\partial \tilde{Y}} \tag{4.11}$$

subject to the boundary condition

$$\frac{\partial \hat{\Phi}^{(1)}}{\partial \tilde{Y}} = -K R_c \mathcal{S}_{\infty 1} \theta \exp\{iK_1 \tilde{X}\} \quad \text{on } \tilde{Y} = 0. \tag{4.12}$$

Substituting (4.10) into (4.11) we obtain

$$\left( \frac{\partial^2}{\partial \tilde{Y}^2} - K_{13}^2 \right) \hat{\Phi}^{(1)} = -K \mathcal{S}_{\infty 2} \exp\{-K_{13} \tilde{Y}\}. \tag{4.13}$$

The general solution for (4.13) is

$$\hat{\Phi}^{(1)} = -(A\tilde{Y} \exp\{-K_{13}\tilde{Y}\} + B \exp\{-K_{13}\tilde{Y}\}), \quad (4.14)$$

where

$$A = \frac{K \mathcal{S}_{\infty 2}}{2K_{13}}.$$

To satisfy the boundary condition on  $N=0$  from (4.12)

$$\left. \frac{\partial \hat{\Phi}^{(1)}}{\partial \tilde{Y}} \right|_{\tilde{Y}=0} = -A + BK_{13} = -KR_c \mathcal{S}_{\infty 1} \theta.$$

Since  $\theta = \tilde{X}/R_c$ , we obtain

$$B = -\frac{\tilde{X} \mathcal{S}_{\infty 1} K}{K_{13}} + \frac{\mathcal{S}_{\infty 2} K}{2K_{13}^2}. \quad (4.15)$$

Since in the source region  $\mathbf{u} = \mathbf{u}_{\infty} - \nabla \Phi$ , the Fourier component for the horizontal component  $u_1$  at  $\tilde{Y}=0$  is obtained from substituting the results (4.14), (4.15) into (4.9a)

$$\mathcal{S}_1 = \mathcal{S}_{\infty 1} + \frac{iK_1 \mathcal{S}_{\infty 2}}{K_{13}} - \frac{\tilde{X} \mathcal{S}_{\infty 1}}{R_c K_{13}} + \frac{iK_1 \mathcal{S}_{\infty 2}}{2R_c K_{13}^2}. \quad (4.16)$$

Hence on the centreline at  $\tilde{x}=0$ , the variances are

$$\overline{|\mathcal{S}_1|^2} = \overline{|\mathcal{S}_{\infty 1}|^2} + \overline{|\mathcal{S}_{\infty 2}|^2} \left( \frac{K_1^2}{K_{13}^2} \right) \left( 1 + \frac{1}{R_c K_{13}} \right), \quad (4.17a)$$

and

$$\overline{|\mathcal{S}_3|^2} = \overline{|\mathcal{S}_{\infty 3}|^2} + \overline{|\mathcal{S}_{\infty 2}|^2} \left( \frac{K_3^2}{K_{13}^2} \right) \left( 1 + \frac{1}{R_c K_{13}} \right). \quad (4.17b)$$

This shows that there is an extra term arising due to curvature, namely  $1/R_c |K_{13}|$ , which is only valid for  $|K_1| > |R_c|^{-1}$  (i.e. for eddies with wavelength less than the length between the peaks and troughs of the undulation).

The normal component as  $\tilde{Y} \rightarrow 0$  is obtained from (4.9a), (4.14) and (4.15), so that the normal velocity relative to the surface is

$$\Delta \mathcal{S}_2 = -\frac{dY}{dX} \mathcal{S}_1 = +\mathcal{S}_{\infty 2} K_{13} \tilde{Y} + \frac{1}{KR_c} (A\tilde{Y} K_{13} - BK_{13} + BK_{13}^2 \tilde{Y}). \quad (4.18a)$$

Thence, using (4.16), the spectrum of the Reynolds stress term relative to the surface is given by

$$\frac{1}{2} \overline{|\mathcal{S}_1^+ \Delta \mathcal{S}_2 + \mathcal{S}_1 \Delta \mathcal{S}_2^+|} \sim -\overline{\mathcal{S}_{\infty 1}^2} \frac{\tilde{X}}{R_c} \tilde{Y} K_{13}. \quad (4.18b)$$

(Note that for isotropic free-stream turbulence  $\overline{|\mathcal{S}_{\infty 1}^+ \mathcal{S}_{\infty 2}|} = 0$ .) Therefore near the crest or trough, since  $K_{13} \sim 1$ ,

$$\overline{u_1 u_2} \sim -\left( \frac{1}{R_c} \right)^2 \overline{u_{\infty 1}^2} \frac{\tilde{X} \tilde{Y}}{R_c} \sim -\left( \frac{1}{R_c} \right)^2 \overline{u_{\infty 1}^2} \frac{\tilde{x} \tilde{y} h (2\pi)^2}{\Lambda^2 L_{\infty}}. \quad (4.19)$$

Note  $\tilde{x} \leq L_{\infty}$  for validity of the analysis. Thence  $\overline{u_1 u_2} \sim -\overline{u_{\infty 1}^2} (L_{\infty} h / \Lambda^2)$ .

From these Fourier coefficients, the variances can be estimated as in §§2 and 3. By inspection of (4.17a) and (4.17b), it follows that the horizontal variances  $\overline{u_1^2}$  and  $\overline{u_3^2}$

(parallel to and perpendicular to the contours of the undulation) are increased by  $O(L_\infty/R_c)$  by the curvature at the bottom of the undulation and reduced at the top of the undulation (where the radius of curvature is negative and the right-hand side of (4.11) changes sign). The Reynolds shear stress  $-\overline{u_1 u_2}$  is negative for  $s > 0$ , and decreases to zero at  $n = 0$ .

These results are qualitatively different to those analysed in §3, where it was shown that gradients of mean Reynolds shear stress normal to a rigid surface develop when the free-stream turbulence is anisotropic, with a finite Reynolds shear stress ( $\overline{u_{\infty 1} u_{\infty 2}} \neq 0$ ). Here we have shown that, over a rigid surface with finite positive or negative radius of curvature, the gradients of the normal and shear Reynolds stresses develop even when the free stream is isotropic.

Another way of looking at this result is to note that for large-scale eddies whose wavelength is much greater than  $R_c$ , the blocking is an average effect. However, since the wavelength is finite, the variations in the curvature of the surface ensure that local blocking induces small local misalignments between the normal to the surface and the major principal axis of the Reynolds stress. These are sufficient to generate a finite shear stress within a distance  $L_\infty$  from the wall. Physical situations can exist where both the anisotropic-slope and isotropic curvature effects operate, as shown in §4.2.

This result can also be understood physically by considering a degenerate form of free-stream ‘turbulence’, consisting of randomly positioned and sparsely distributed line vortices with initial orientation (a) parallel and (b) perpendicular to the contours of the undulating surface. Because of their assumed sparse spacing, they interact only with the surface. For both type (a) and type (b) the blocking effect of the wall is greater/less at the troughs/peaks with correspondingly greater/less values of  $\overline{u_1^2}$  near the surface.

#### 4.2. Calculation of the mean velocity field over the undulating surface

It is assumed that in (2.5c) the integral scale of the turbulence  $L_\infty$  is small compared to the wavelength  $\Lambda$  and the radius of curvature ( $\Lambda^2/h$ ), and that the slope is small (i.e.  $h/\Lambda \ll 1$ ). Then the integral of the mean vorticity  $\Omega_z$  in the source layer is given by the mean velocity  $\mathbf{U} = \tilde{\mathbf{U}} = (\tilde{U}, \tilde{V}, 0)$  (outside the viscous layer, viscous stresses are negligible):

$$\frac{\partial}{\partial t} \int_{\tilde{y}}^{\infty} \Omega_z \, d\tilde{y} = + \frac{\partial}{\partial t} \left\{ \tilde{U} \left( \frac{\tilde{y}}{L_\infty} \right) - \tilde{U} \left( \frac{\tilde{y}}{L_\infty} \rightarrow \infty \right) \right\} = \left( -\frac{\partial}{\partial \tilde{x}} \overline{u_1^2} + \frac{\partial}{\partial \tilde{y}} (-\overline{u_1 u_2}) \right) \left( \frac{\tilde{y}}{L_\infty} \right). \quad (4.20)$$

Note that from (4.18) and (4.17), the second term on the right-hand side of (4.20), the Reynolds stress term (of order  $v_\infty^2 ((2\pi)^2 h/\Lambda^2)$ ), is larger than the normal stress term,  $v_\infty^2 (2\pi) h L_\infty / \Lambda^3$ . Also, we have shown in the previous section that for  $L_\infty \geq \tilde{x} > 0$  and  $0 < \tilde{y} \ll L_\infty$ ,

$$\frac{\partial}{\partial \tilde{x}} \overline{u_1^2} < 0, \quad \frac{\partial (-\overline{u_1 u_2})}{\partial \tilde{y}} > 0. \quad (4.21a)$$

However, for  $\tilde{y} \geq L_\infty$ ,  $-\overline{u_1 u_2} \rightarrow 0$ , so that  $(\partial/\partial \tilde{y})(-\overline{u_1 u_2})$  changes sign within  $L_\infty$ , being positive near the surface and negative away from the surface. It follows that the secondary flow  $\tilde{U}(\tilde{y})$  induced by the shear stress has approximately zero net flux, and is therefore restricted to the surface layer  $\tilde{y} < L_\infty$ . However, the smaller horizontal gradient in normal stress  $\partial \overline{u_1^2} / \partial \tilde{x}$  has the same sign throughout the source layer and

therefore drives a mean velocity  $\tilde{V}$  within  $L_\infty$  with a finite flux. This in turn sets up a return flow outside  $L_\infty$ .

Hence in the source layer,

$$\frac{\partial}{\partial t} \left\{ U \left( \frac{\tilde{y}}{L_\infty} \rightarrow 0 \right) - U \left( \frac{\tilde{y}}{L_\infty} \rightarrow \infty \right) \right\} > 0 \text{ for } \tilde{x} > 0, \tag{4.21b}$$

$$< 0 \text{ for } \tilde{x} < 0.$$

Note that the other components of  $\mathbf{\Omega}$  are zero in this two-dimensional mean flow. Note also that

$$\tilde{U} \sim \nu v_\infty^2 (2\pi)^2 h / \Lambda^2, \tag{4.21c}$$

while

$$\tilde{V} \sim \nu v_\infty^2 (2\pi)^3 h L_\infty / \Lambda^3, \tag{4.21d}$$

Thus the mean velocity field parallel to the surface varies along the surface. By continuity, it follows that a mean velocity field  $\mathbf{U}^{(w)}$  is set up where  $\tilde{y} > L_\infty$ , with flow into and out of the source layer driven by the finite flux of  $\tilde{V}$ . This external field in the ‘wave’ layer extends over a distance of order of the wavelength  $\Lambda (= 2\pi/k)$  normal to the surface. The mean flow here is initially irrotational since the turbulence is homogeneous outside the source layer, and the right-hand side of (2.5c) is zero. Since  $\nabla \cdot \mathbf{U}^{(w)} = 0$  and  $\nabla \wedge \mathbf{U}^{(w)} = 0$ ,  $\mathbf{U}^{(w)}$  can be expressed in terms of a streamfunction  $\Psi^{(w)}$ ,

$$\mathbf{U}^{(w)} = \left( -\frac{\partial \Psi^{(w)}}{\partial y}, \frac{\partial \Psi^{(w)}}{\partial x}, 0 \right), \tag{4.22a}$$

where  $\Psi^{(w)}$  satisfies Laplace’s equation, i.e.

$$\frac{\partial^2 \Psi^{(w)}}{\partial x^2} + \frac{\partial^2 \Psi^{(w)}}{\partial y^2} = 0. \tag{4.22b}$$

Since

$$\int_{y=y_s}^\infty U_1 \, dy = 0, \tag{4.22c}$$

by continuity, as  $y/\Lambda \rightarrow 0$  and since  $\Psi^{(w)} \rightarrow 0$  as  $y \rightarrow \infty$ ,

$$\Psi^{(w)}(x, 0) = - \int_0^\infty \tilde{U} \, d\tilde{y}. \tag{4.22d}$$

However,  $(\partial/\partial \tilde{x}) \overline{u_1^2} < 0$  for  $0 < \tilde{y}$ . Hence  $\int_0^\infty (\partial/\partial \tilde{x}) \overline{u_1^2} \, d\tilde{y} < 0$ , although  $\int_0^\infty (\partial/\partial \tilde{y})(-\overline{u_1 u_2}) \, d\tilde{y} \rightarrow 0$ .

The mean velocity component in the source layer parallel to the surface  $\tilde{V}$  which is driven by the normal stress is zero at  $\tilde{x} = 0$ ,  $\tilde{x} = \pm \Lambda/2$ . Since it decays with  $y$  over a distance of order  $L_\infty$ , its approximate form is

$$\tilde{V} \simeq \tilde{V}_{mx} \exp\{-n/L_\infty\} \sin kx, \tag{4.22e}$$

where

$$\tilde{V}_{mx} \sim \nu v_\infty^2 (2\pi h L_\infty / \Lambda^3). \tag{4.22f}$$

(This is the leading term in a Fourier series expansion.) Therefore,

$$\int_0^\infty \tilde{V} \, d\tilde{y} \simeq \tilde{V}_{mx} L_\infty \sin kx. \tag{4.23}$$

The solution for  $\Psi$  that satisfies (4.22b) is

$$\Psi^{(w)} = -\tilde{V}_{mx} L_\infty \sin kx \exp\{-ky\}. \quad (4.24)$$

Thus the mean vertical velocity in the external wave layer is

$$U_2^{(w)} = -2\pi\tilde{V}_{mx} \frac{L_\infty}{\Lambda} \exp\{-ky\}(\sin kx, \cos kx, 0), \quad (4.25)$$

so that  $U_2^{(w)}$  is negative near the troughs and positive over the peaks, while the horizontal component is negative on the upslopes (in a coordinate system where  $dy_s/dx > 0$ ) and positive on the down (negative) slopes. Note that from (4.25) the vertical extent of the wave layer is of order  $\Lambda/\pi$ . Here,  $U^{(w)}$  decreases to 10% of the maximum value, which is given by

$$|U^{(w)}| \sim \frac{L_\infty}{\Lambda} \tilde{V}_{mx}. \quad (4.26)$$

Thus,  $U^{(w)}$  in the outer wave layer is much smaller than the mean velocity in the source layer, since  $L_\infty/\Lambda \ll 1$ .

In many geophysical situations where the large-scale turbulence above the undulating surface is anisotropic, e.g. caused by thermal convection, mean flows can also be generated up and down the slope by the anisotropy-slope mechanism analysed in §3.

Note that, as in the analysis of §3, the mean velocity of the secondary flow reaches an approximately steady state, determined either by the time scale of the mean recirculating flow,  $T_c = \Lambda/\tilde{U}_{mx}$  or by  $T_L \sim L_\infty/v'_\infty$ , whichever is the smaller. Therefore, from (4.20) and (4.22f),

$$\tilde{U}_{mx}(t \sim T_c) \sim \left(\frac{L_\infty h}{\Lambda^2}\right)^{1/2} v'_\infty, \quad (4.27)$$

where  $\tilde{U}_{mx}(t \sim T_c) \sim v'_\infty(2\pi h/\Lambda)^{1/2}$  (only if  $T_c < \tau$ ) (cf. Davidson & Hunt 1987).

## 5. Experimental observations

To test the theoretical predictions that secondary flows can be induced by the distortion of turbulence as it impacts onto surfaces without mean shear, two qualitative laboratory experiments are described. The first examines the formation of secondary motion generated by anisotropic (axisymmetric) turbulence near a flat surface, when the orientation of the principal axes of the turbulence are neither perpendicular nor parallel to the surface. The second is concerned with the formation of secondary flows when isotropic free-stream turbulence is distorted by an undulating surface (Wong 1985).

Both experiments were conducted inside a mixing tank at the Department of Applied Mathematics and Theoretical Physics laboratory in Cambridge with quasi-homogeneous turbulence generated by oscillating grids, one for anisotropic and the other for isotropic turbulence. The velocity of the secondary flow is of the order of magnitude of the r.m.s. of the longitudinal fluctuating velocity component in the free stream,  $v'_\infty$ , and is studied using the flow-visualization techniques described below.

The installation used was based on that constructed by Thompson & Turner (1975). The mixing tank used was a cuboid box made of 0.95 cm Perspex sheet and measuring internally 25.4 cm  $\times$  25.4 cm by 45.7 cm deep. The grids were attached to a vertical stainless steel rod of 0.48 cm diameter which passed through bearings. The rod was

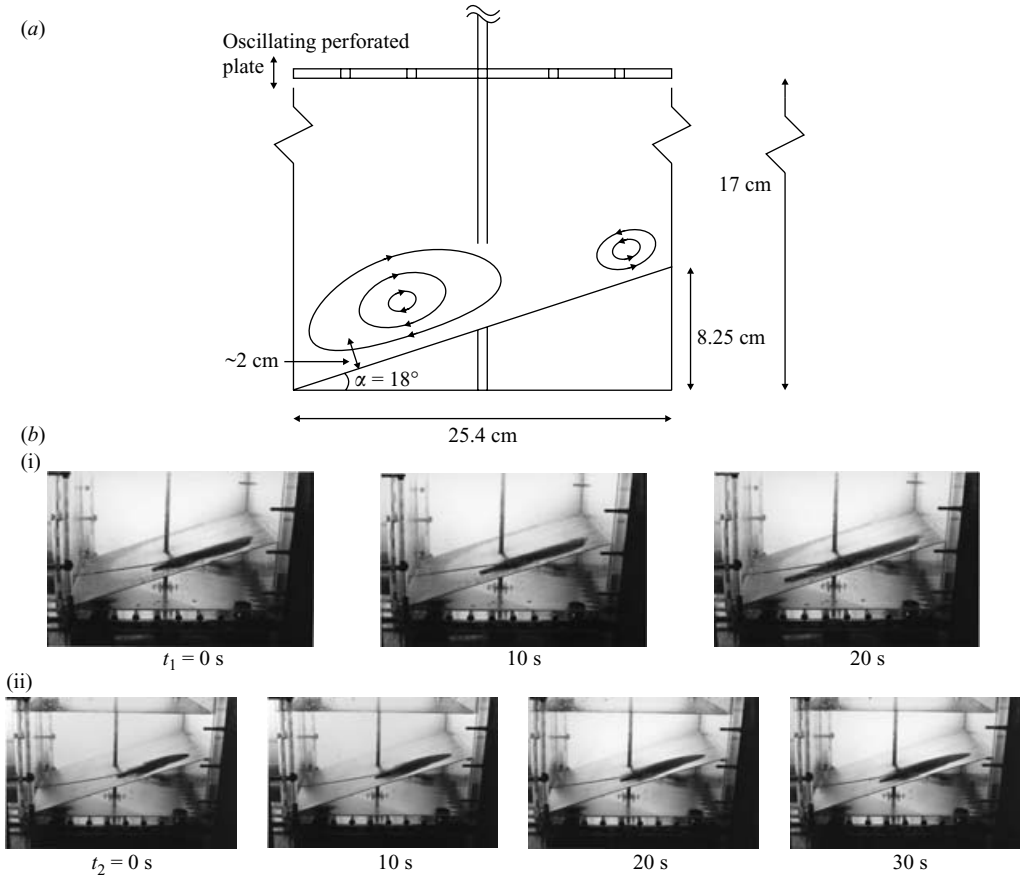


FIGURE 9. (a) Pattern of secondary flow over a flat plate surface owing to the distortion of axisymmetric turbulence. (b) (i) One set of dye experiments showing the existence of secondary flow down the inclined flat surface. The frequency is  $f = 5.5$  Hz and stroke is 0.8 cm. (ii) Control experiment showing the displacement of slightly buoyant dye over the flat surface in still water. The time interval is indicated in each case.

located at the top and bottom of the tank. The grids were oscillated vertically by a variable throw crank in the range 0.25 to 1.5 cm attached to the rod and driven through a 15:1 worm gear by a 240 V alternating current electric motor. The speed of the motor was varied by using a rheostat to reduce the voltage and measured by a strobe disk designed to exploit the 50 cycles  $s^{-1}$  oscillation of an electric light. This enabled the frequency of the grid (between 5.5 and 11 Hz) to be kept within  $\pm 3\%$  of its mean value. The type and size of the grid and its position above the bottom of the tank are described below for each experiment (see figure 9).

### 5.1. Anisotropic turbulence over a plane surface

In the first experiment, the stirring grid is a perforated Perspex plate with holes of diameter 1.7 cm uniformly distributed over the plate so that the solidity of the plate is 60%. This produces turbulence fluctuations whose vertical component  $(\overline{u_2^2})^{1/2}$  is about 20% greater than  $(\overline{u_1^2})^{1/2}$ ,  $(\overline{u_3^2})^{1/2}$  (Townsend 1976). The grid measures 25 cm  $\times$  25 cm by 1 cm thick and was placed about 17 cm above the bottom of the tank. Below the

grid was an aluminium flat plate inclined at  $18^\circ$  to the horizontal with its top end about 8.75 cm below the perforated plate. In this way, the axis of the axisymmetric turbulence, unit vector  $e$ , created by the oscillating grid is at an acute angle (about  $18^\circ$ ) to the normal  $n$  to the plate.

Figure 9 shows a typical result for the flow-visualization experiments (using dye). The exposure time is 4 s. The mean circulation occurred when the frequency was above 7 Hz. In figure 9(b) (i) we see the dye front moving from right to left driven by mean flow over the surface. Figure 9(b) (ii) shows the control experiment in still water to check the effect of buoyancy on dye observation. We can confirm that the dye hardly moves in the control experiment. Therefore, we can conclude that the mean flow is generated over the surface by the blocking of anisotropic turbulence. There are two sets of secondary flows over the inclined plane which were approximately in a steady state (see the sketch in figure 9a). In the stronger and larger one which dominates most of the region between the inclined plane and the oscillating plate, the mean flow moves downwards along the plane at a velocity of about  $1/3 \text{ cm s}^{-1}$  with a layer of thickness  $2 \text{ cm} \sim 2L_\infty$ , except near the upper end where the weaker one rotates in the opposite sense to the stronger one. This is consistent with our theory, equation (3.16) for  $R \simeq 1.2$  and  $\alpha \simeq 18^\circ$ . Since in the experiment  $U \sim v'_{\infty}$ ,  $\sin 2\alpha(1 - 1/R) \sim 0.1$ . This means that in the theoretical model, the coefficient  $u'_{\infty s}/v'_{\infty} \simeq u'_{\infty s}/U$  (which determines the nonlinear interaction of the flow) is small ( $\sim 1/10$ ) – as in steady-state shear flows. Since the region at the upper end of the plate is close to the grid, the normal stress in the axial ( $y$ ) direction may be smaller than for the other components. Hence the smaller secondary-flow eddy moves upwards along the plane in this region.

The observation from this experiment is consistent with the theoretical prediction that secondary flow exists as a consequence of the distortion of eccentrically orientated axisymmetric free-stream turbulence above a flat inclined surface without mean shear.

A control experiment was performed on a flat plate parallel to an isotropic grid (described in §2). No mean flow was observed.

### 5.2. Isotropic turbulence over an undulating surface

In the second experiment, the surface consists of a fixed undulating surface placed inside a mixing tank with homogeneous turbulence created over the whole surface by an oscillating grid. Since the secondary flow over low-amplitude surface undulation (where  $h \ll L_\infty$ ) would be too weak to be visualized, in the experiment, the amplitude of the undulating surface was larger than those assumed in the theory of §4 (where  $h \ll L_\infty$ ).

The grids were made of square bars having a mesh size  $M = 5 \text{ cm}$  and a bar width  $d = 1 \text{ cm}$ , i.e. a solidity of 0.36. The grids were placed at about 11 cm above the bottom of the tank. The frequency of the stroke in this experiment was greater than 7 Hz. An undulatory surface made of polycarbonate (plastic) was fixed at the bottom of the tank, with wavelength  $\Lambda \simeq 7 \text{ cm}$  and amplitude  $h \simeq 1 \text{ cm}$ . According to the experimental data of Thompson & Turner (1975), the integral length scale  $L_\infty$  varies linearly with the distance away from the grid. For the above arrangement,  $L_\infty \sim 1 \text{ cm}$ , so that  $h/L_\infty \simeq 1$  and  $L_\infty/\Lambda \sim 1/7$ . Also, from Thompson & Turner (1975), the r.m.s. fluctuating velocity  $v'_{\infty}$  is of the order 0.2 to  $0.5 \text{ cm s}^{-1}$ . This is the appropriate range for flow visualization using dye or aluminium flakes. Note that the Reynolds number  $Re$  of the turbulence ( $v'_{\infty} L_\infty/\nu$ ) throughout the depth is approximately constant. The range of  $Re$  in our experiments was between 20 and 50. The flakes indicated a mean flow pattern centred on the undulation. However, by using blue dye it was possible to observe the direction of the mean flow, if any.

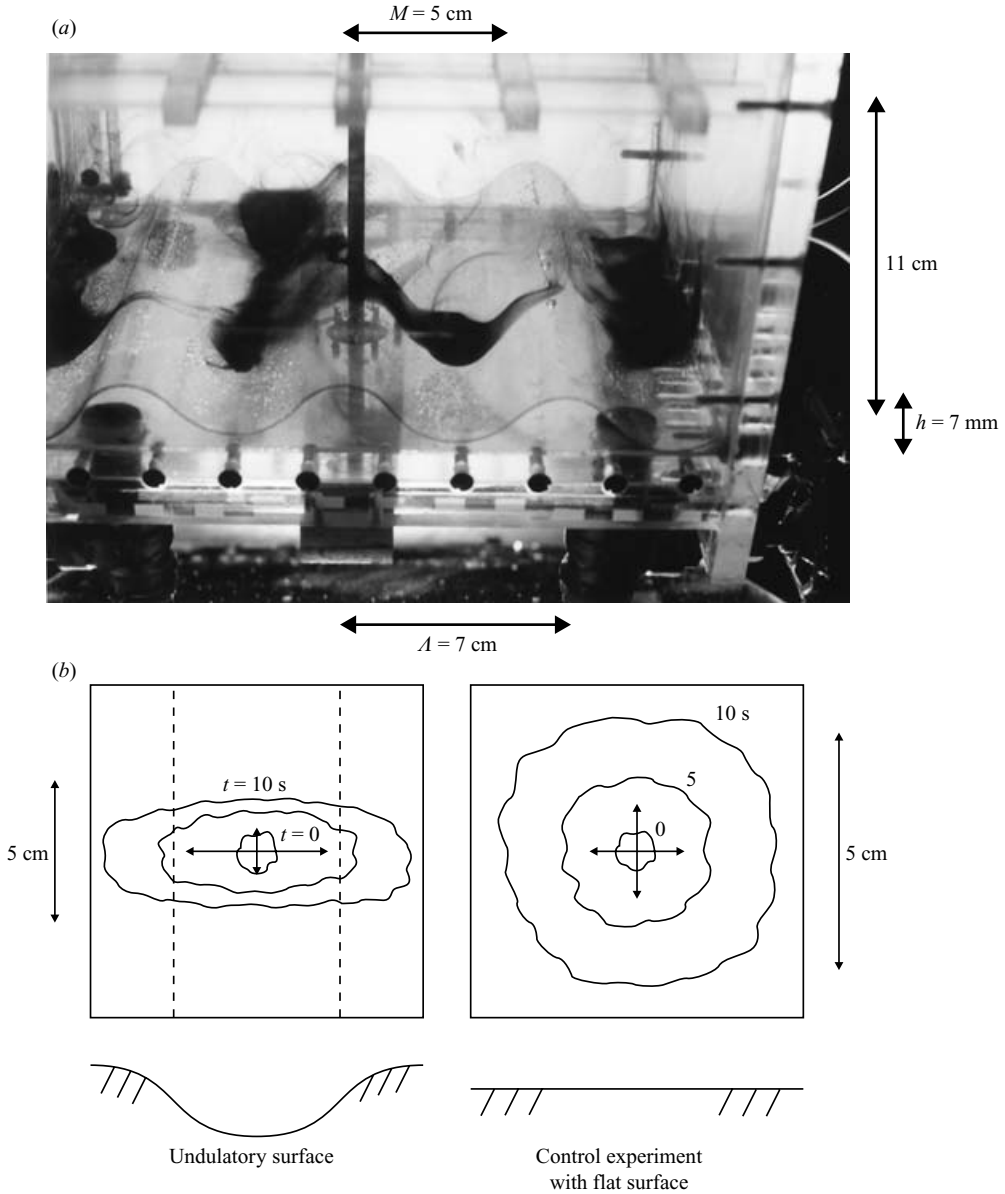


FIGURE 10. Isotropic grid turbulence above an undulating surface. (a) A flow-visualization experiment using food dye showing the pattern of the secondary flow and the mean-circulation following dye release in the trough. 10 s ( $\approx 20L_\infty/v'_\infty$ ) after release. The frequency is 11 Hz and stroke is 0.25 cm. (b) Comparison between a flat plate and an undulatory surface on the dispersion of dye near the surface.

Figure 10 shows a typical result for this experiment showing how a steady mean flow was set up, with mean flow down into the troughs and up from the crests. In figure 10(a), the dye (black region) was initially released in the trough. The direction of the mean flow near the crests is clearly upward and away from the crests. The depth of the wave-layer with significant secondary flow is about 2 to 3 cm, as expected, being 1/3 of the magnitude of  $\Lambda$ , and its velocity is between 0.3 and 0.8 cm s<sup>-1</sup>, which is the same order as  $v'_\infty(2\pi h/\Lambda)$  as predicted by (4.27). A further confirmation in

figure 10(b) shows how dye released in the trough moves up the slopes and is elongated, whereas over a flat surface it spreads isotropically.

These experiments showed that the secondary flow exists as a result of the distortion of isotropic free-stream turbulence above an undulating surface without mean shear. The results agree qualitatively with the theoretical predictions made in this paper on the magnitude and form of the secondary flow. The tendency of shear-free turbulence to generate a mean flow over an uneven surface towards the locations with higher positive curvature (inwards) is consistent with the experiments of Gessner & Emery (1981).

## 6. Conclusions

First, we have shown how the form of the spectrum and the degree and form of anisotropy of shear-free turbulence affect the turbulence on a flat plate using linear rapid distortion theory. The main results from this theoretical study supported by laboratory experiments can be summarized as follows.

(a) The effects of blocking on the variances extend farther from the plate for a low-Reynolds-number spectrum (i.e. with exponential decay), in the sense that the normal velocity fluctuations decrease more and streamwise and spanwise velocity fluctuations increase more than those at high Reynolds numbers. The turbulence kinetic energy is everywhere slightly greater. However, the reduction of the streamwise integral length scale of vertical velocity fluctuation is less with a typical low-Reynolds-number spectrum. In this case,  ${}^xL_{22}$  approaches the limit  $0.4 L_\infty$  near the surface, whereas  ${}^xL_{22} \propto Y$  and approaches to zero in high Reynolds number turbulence. (This is direct evidence for recommending that turbulence models should have different parameterizations depending on the form of the spectrum, e.g. Launder & Spalding 1972). Note that at low Reynolds number, the viscous layer is much larger. In fact, when  $Re \leq 50$  it dominates the source layer and no amplification of  $u_1^2$  is expected, as shown by the profile of  $\overline{u_1^2}$  in the viscous layer obtained by this study. This is consistent with McDougall's (1979) mixing-box experiment.

(b) With impingement of turbulence onto a flat surface, Reynolds stress gradients are generated normal to the surface over a distance of order  $L_\infty$  if the turbulence is anisotropic and if the principal axes are orientated at an acute angle  $\alpha$  to the surface. Then the curl of the Reynolds stress gradients is non-zero (in other words, a gradient of a Reynolds stress is generated which does not occur with isotropic free-stream turbulence). This drives a mean secondary flow which grows near the surface linearly with time  $t$ . Its maximum value occurs at the top of the viscous layer and decreases with distance from the surface  $y$ .

(c) Nonlinear mechanisms control the growth of the mean secondary flow  $U^*$  so that it is of the order of the r.m.s. velocity of the free stream  $v'_\infty$ .

Secondly, we have shown how homogeneous free-stream turbulence is distorted by a long-wavelength undulatory rigid surface. Reynolds stress gradients are generated that generate mean velocity gradients. In an analysis using rapid distortion theory, three asymptotic layers were identified over the wavy surface. In the middle 'source' layer extending a distance  $L_\infty$  from the surface, mean vorticity is driven by the Reynolds stress gradients. If the wavelength  $\Lambda$  is greater than  $L_\infty$ , a recirculating mean flow is driven over the length scale  $\Lambda$  of the undulation. This may well have wider implications in geophysical and engineering flows, especially at gas-liquid interfaces and at erodible solid interfaces (e.g. Bagnold 1941; Feltham *et al.* 2002). The results shown here are consistent with the 'mixing-box' laboratory experiment of turbulence above an undulating surface (Wong 1985) and direct numerical simulation of convective motion over a wavy terrain by Krettenauer & Schumann (1992).

In a turbulent boundary layer, recirculating flows with streamwise vorticity are generated by the anisotropy of the turbulence interacting with the surface (Townsend 1976). If the lateral wavelength of these structures ( $\sim 7 \times$  boundary-layer depth) is of the same order as that of surface undulations aligned with the flow, the wave-modulated blocking mechanism could amplify the shear structures.

H.W. acknowledges a research student's grant from SERC. We thank for D. Cheesely and D. Lippman for help with the laboratory experiments. K.N. thanks the Japanese Ministry of Education, Culture, Sports, Science and Technology and Center of Excellence for Research and Education on Complex Functional Mechanical Systems (COE program of the Ministry of Education, Culture, Sports, Science and Technology, Japan) for his visiting fellowship to University College London (UCL) and University of Cambridge during 2002–2003. K.N. also thanks S. Komori for help with his visiting fellowship. J.C.R.H. acknowledges support by NERC to CPOM at UCL. We are grateful for the referees' constructive comments.

**Appendix. Source-layer profiles of variances and co-variances for turbulence near a flat surface when the axisymmetric principal axis is at an angle  $\alpha$  to the surface**

$$\begin{aligned} \overline{u_1^2}/\overline{u_{\infty 1a}^2} &= 1 - \sin^2 \alpha \left(1 - \frac{1}{R}\right) + \frac{1}{4} \left(1 - \frac{2}{R}\right) Y \left[-\frac{Y}{\lambda_1} \exp\left\{-\frac{Y^2}{4\lambda_1}\right\}\right. \\ &\quad + \left(\frac{\pi}{\lambda_1}\right)^{1/2} \left(1 + \frac{Y^2}{2\lambda_1}\right) \operatorname{erfc}\left\{\frac{1}{2}\lambda_1^{-1/2}Y\right\} \left. + \frac{1}{4} \left(1 - \frac{2}{R}\right) \left[-2\left(\frac{Y^2}{\lambda_1} + 1\right)\right.\right. \\ &\quad + \left(\frac{\pi}{\lambda_1}\right)^{1/2} Y \left(3 + \frac{2Y^2}{\lambda_1}\right) \exp\left\{\frac{Y^2}{\lambda_1}\right\} \operatorname{erfc}\left\{\lambda_1^{-1/2}Y\right\} \left. \right] \\ &\quad + \frac{1}{2} \left(1 - \frac{1}{R}\right) Y \left[\frac{Y}{\lambda_2} \exp\left\{-\frac{Y^2}{4\lambda_2}\right\} - \left(\frac{\pi}{\lambda_2}\right)^{1/2} \left(1 + \frac{Y^2}{2\lambda_2}\right) \operatorname{erfc}\left\{\frac{1}{2}\lambda_2^{-1/2}Y\right\}\right] \\ &\quad + \frac{1}{8}(3 + \sin^2 \alpha) \left(1 - \frac{1}{R}\right) \left[2\left(\frac{Y^2}{\lambda_2} + 1\right)\right. \\ &\quad \left. - \left(\frac{\pi}{\lambda_2}\right)^{1/2} Y \left(3 + \frac{2Y^2}{\lambda_2}\right) \exp\left\{\frac{Y^2}{\lambda_2}\right\} \operatorname{erfc}\left\{\lambda_2^{-1/2}Y\right\}\right] \end{aligned} \tag{A 1}$$

$$\begin{aligned} \overline{u_2^2}/\overline{u_{\infty 1a}^2} &= \frac{1}{R} + \sin^2 \alpha \left(1 - \frac{1}{R}\right) + \left(1 - \frac{2}{R}\right) \left[2\left(\frac{Y^2}{4\lambda_1} + 1\right) \exp\left\{-\frac{Y^2}{4\lambda_1}\right\}\right. \\ &\quad - \frac{1}{2} \left(\frac{\pi}{\lambda_1}\right)^{1/2} Y \left(3 + \frac{Y^2}{2\lambda_1}\right) \operatorname{erfc}\left\{\frac{1}{2}\lambda_1^{-1/2}Y\right\} \left. + \left(1 - \frac{2}{R}\right) \left[-\left(\frac{Y^2}{\lambda_1} + 1\right)\right.\right. \\ &\quad + \frac{1}{2} \left(\frac{\pi}{\lambda_1}\right)^{1/2} Y \left(3 + \frac{2Y^2}{\lambda_1}\right) \exp\left\{\frac{Y^2}{\lambda_1}\right\} \operatorname{erfc}\left\{\lambda_1^{-1/2}Y\right\} \left. \right] \\ &\quad + (1 + \sin^2 \alpha) \left(1 - \frac{1}{R}\right) \left[-2\left(\frac{Y^2}{4\lambda_2} + 1\right) \exp\left\{-\frac{Y^2}{4\lambda_2}\right\}\right. \\ &\quad + \frac{1}{2} \left(\frac{\pi}{\lambda_2}\right)^{1/2} Y \left(3 + \frac{Y^2}{2\lambda_2}\right) \operatorname{erfc}\left\{\frac{1}{2}\lambda_2^{-1/2}Y\right\} \left. + (1 + \sin^2 \alpha) \left(1 - \frac{1}{R}\right)\right. \\ &\quad \left. \times \left[\left(\frac{Y^2}{\lambda_2} + 1\right) - \frac{1}{2} \left(\frac{\pi}{\lambda_2}\right)^{1/2} Y \left(3 + \frac{2Y^2}{\lambda_2}\right) \exp\left\{\frac{Y^2}{\lambda_2}\right\} \operatorname{erfc}\left\{\lambda_2^{-1/2}Y\right\}\right] \end{aligned} \tag{A 2}$$

$$\begin{aligned}
\overline{u_3^2/u_{\infty 1a}^2} &= \frac{1}{R} + \frac{1}{4} \left(1 - \frac{2}{R}\right) Y \left[ -\frac{Y}{\lambda_1} \exp \left\{ -\frac{Y^2}{4\lambda_1} \right\} \right. \\
&+ \left. \left( \frac{\pi}{\lambda_1} \right)^{1/2} \left( 1 + \frac{Y^2}{2\lambda_1} \right) \operatorname{erfc} \left\{ \frac{1}{2} \lambda_1^{-1/2} Y \right\} \right] + \frac{1}{4} \left(1 - \frac{2}{R}\right) \left[ -2 \left( \frac{Y^2}{\lambda_1} + 1 \right) \right. \\
&+ \left. \left( \frac{\pi}{\lambda_1} \right)^{1/2} Y \left( 3 + \frac{2Y^2}{\lambda_1} \right) \exp \left\{ \frac{Y^2}{\lambda_1} \right\} \operatorname{erfc} \left\{ \lambda_1^{-1/2} Y \right\} \right] \\
&+ \frac{\sin^2 \alpha}{2} \left(1 - \frac{1}{R}\right) Y \left[ \frac{Y}{\lambda_2} \exp \left\{ -\frac{Y^2}{4\lambda_2} \right\} \right. \\
&- \left. \left( \frac{\pi}{\lambda_2} \right)^{1/2} \left( 1 + \frac{Y^2}{2\lambda_2} \right) \operatorname{erfc} \left\{ \frac{1}{2} \lambda_2^{-1/2} Y \right\} \right] + \frac{1}{8} (1 + 3 \sin^2 \alpha) \left(1 - \frac{1}{R}\right) \\
&\times \left[ 2 \left( \frac{Y^2}{\lambda_2} + 1 \right) - \left( \frac{\pi}{\lambda_2} \right)^{1/2} Y \left( 3 + \frac{2Y^2}{\lambda_2} \right) \exp \left\{ \frac{Y^2}{\lambda_2} \right\} \operatorname{erfc} \left\{ \lambda_2^{-1/2} Y \right\} \right] \quad (\text{A } 3)
\end{aligned}$$

$$\begin{aligned}
\overline{u_1 u_2 / u_{\infty 1a}^2} &= \frac{1}{2} \sin 2\alpha \left(1 - \frac{1}{R}\right) \left[ 1 - \left( \frac{Y^2}{4\lambda_2} + 1 \right) \exp \left\{ -\frac{Y^2}{4\lambda_2} \right\} \right. \\
&+ \left. \frac{1}{4} \left( \frac{\pi}{\lambda_2} \right)^{1/2} Y \left( 3 + \frac{Y^2}{2\lambda_2} \right) \operatorname{erfc} \left\{ \frac{1}{2} \lambda_2^{-1/2} Y \right\} \right] \quad (\text{A } 4)
\end{aligned}$$

$$\overline{u_2 u_3 / u_{\infty 1a}^2} = \overline{u_3 u_1 / u_{\infty 1a}^2} = 0 \quad (\text{A } 5)$$

## REFERENCES

- BAGNOLD, R. A. 1941 *The Physics of Blown Sand and Desert Dunes*. Chapman & Hall.
- BATCHELOR, G. K. 1953 *Homogeneous Turbulence*. Cambridge University Press.
- BRUMLEY, B. H. & JIRKA, G. H. 1987 Near-surface turbulence in a grid-stirred tank. *J. Fluid Mech.* **183**, 235–263.
- CAMBON, C. 2001 Turbulence and vortex structures in rotating and stratified flows. *Eur. J. Mech. B/Fluids* **20**, 489–510.
- CAMBON, C. & TEISSÈDRE, C. 1985 Application des harmoniques sphériques à la représentation et au calcul des grandeurs cinématiques en turbulence homogène anisotrope. *C. R. Acad. Sci. Paris II* **301**, 65–68.
- CARLOTTI, P. 2001 Distorted turbulence near rigid boundaries. PhD thesis, University of Cambridge.
- CRAYA, A. 1958 Contribution à l'analyse de la turbulence associée à des vitesses moyennes. *Pub. Sci. Tech. du Ministère de l'Air (France)*, no. 345.
- DAVIDSON, P. A. & HUNT, J. C. R. 1987 Swirling recirculating flow in a liquid metal column generated by a rotating magnetic field. *J. Fluid Mech.* **185**, 67–106.
- DURBIN, P. A. 1993 A Reynolds stress model for near-wall turbulence. *J. Fluid Mech.* **249**, 465–498.
- FELTHAM, D. L., WORSTER, M. G. & WETTLAUFER, J. S. 2002 The influence of ocean flow on newly-forming sea ice. *J. Geophys. Res.* **107**, C2, 1–10.
- FERNANDO, H. J. S. & DE SILVA, I. P. D. 1993 Note on secondary flows in oscillating-grid, mixing-box experiments. *Phys. Fluids A* **5**, 1849–1851.
- GESSNER, F. B. & EMERY, A. F. 1981 The numerical prediction of developing turbulent flow in rectangular ducts. *J. Fluids Engng* **103**, 445–455.
- GIBSON, M. M. & LAUNDER, B. E. 1978 Ground effects on pressure fluctuations in the atmospheric boundary layer. *J. Fluid Mech.* **86**, 491–511.
- HANNOUN, I. A., FERNANDO, H. J. S. & LIST, E. J. 1988 Turbulence structure near a sharp density interface. *J. Fluid Mech.* **189**, 189–209.
- HERRING, J. R. 1974 Approach of axisymmetric turbulence to isotropy. *Phys. Fluids* **17**, 859–872.
- HÖGSTRÖM, U., HUNT, J. C. R. & SMEDMAN, A. 2002 Theory and measurements for turbulence spectra and variances in the near neutral surface layer. *Boundary Layer Met.* **103**, 101–124.

- HUNT, J. C. R. 1984 Turbulence structure in thermal convection and shear-free boundary layers. *J. Fluid Mech.* **138**, 161–184.
- HUNT, J. C. R. & CARRUTHERS, D. J. 1990 Rapid distortion theory and the ‘problems’ of turbulence. *J. Fluid Mech.* **212**, 497–532.
- HUNT, J. C. R. & GRAHAM, J. M. R. 1978 Free-stream turbulence near plane boundaries. *J. Fluid Mech.* **84**, 209–235.
- HUNT, J. C. R. & MORRISON, J. F. 2000 Eddy structure in turbulent boundary layers. *Eur. J. Mech. B/Fluids* **19**, 673–694.
- KAIMAL, J. C., WYNGAARD, J. C., IZUMI, Y. & COTE, O. R. 1972 Spectral characteristics of surface-layer turbulence. *Q. J. R. Met. Soc.* **98**, 563–589.
- KIT, E. L. G., STRANG, E. J. & FERNANDO, H. J. S. 1997 Measurement of turbulence near shear-free density interfaces. *J. Fluid Mech.* **334**, 293–314.
- KRETTENAUER, K. & SCHUMANN, U. 1992 Numerical simulation of turbulent convection over wavy terrain. *J. Fluid Mech.* **237**, 261–299.
- KRISHNAMURTI, R. & HOWARD, L. N. 1981 Large-scale flow generation in turbulent convection. *Proc. Natl Acad. Sci. USA* **78**, 1981–1985.
- LAUNDER, B. E. & SPALDING, D. B. 1972 *Mathematical Models of Turbulence*. Academic Press.
- LAUNDER, B. E. & YING, W. G. 1972 Secondary flows in ducts of square cross-section. *J. Fluid Mech.* **54**, 289–295.
- MCDUGALL, T. J. 1979 Measurements of turbulence in a zero-mean-shear mixed layer. *J. Fluid Mech.* **94**, 409–431.
- MAGNAUDET, J. 2003 High-Reynolds-number turbulence in a shear-free boundary layer: revisiting the Hunt–Graham theory. *J. Fluid Mech.* **484**, 167–196.
- MANN, J. 1994 The spatial structure of neutral atmospheric surface-layer turbulence. *J. Fluid Mech.* **273**, 141–168.
- OWINOH, A. Z., HUNT, J. C. R., ORR, A. & KLEIN, R. 2004 Dynamics of flow over a low hill caused by change in surface heat flux. *Eur. Geophys. Soc. 27th General Assembly, Nice, France*.
- PEROT, B. & MOIN, P. 1995 Shear-free turbulent boundary layers. Part 1. Physical insights into near-wall turbulence. *J. Fluid Mech.* **295**, 199–227.
- PLATE, E. J., FEDOROVICH, E., VIEGAS, D. X. & WYNGAARD, J. C. (Eds.) 1998 *Buoyant Convection in Geophysical Flows*, 265–290. Kluwer.
- PRANDTL, L. 1956 *Essentials of Fluid Dynamics*. Dover.
- PRIGOGINE, I. & STENGERS, I. 1984 *Order out of Chaos*. Heinemann.
- SREENIVASAN, K. R. & NARASIMHA, R. 1978 Rapid distortion of axisymmetric turbulence. *J. Fluid Mech.* **84**, 497–516.
- TENNEKES, H. & LUMLEY, J. L. 1972 *A First Course in Turbulence*. MIT Press.
- THOMAS, N. H. & HANCOCK, P. E. 1977 Grid turbulence near a moving wall. *J. Fluid Mech.* **82**, 481–496.
- THOMPSON, S. M. & TURNER, J. S. 1975 Mixing across an interface due to turbulence generated by an oscillating grid. *J. Fluid Mech.* **67**, 349–368.
- TOWNSEND, A. A. 1976 *The Structure of Turbulent Shear Flow*, 2nd edn. Cambridge University Press.
- UZKAN, T. & REYNOLDS, W. C. 1967 A shear-free turbulent boundary layer. *J. Fluid Mech.* **28**, 803–821.
- WONG, H. Y. W. 1985 Shear-free turbulence and secondary flow near angled and curved surfaces. PhD thesis, University of Cambridge.
- WOOD, D. H. & BRADSHAW, P. 1984 A turbulent mixing layer constrained by a solid surface. Part 2. Measurements in the wall-bounded flow. *J. Fluid Mech.* **139**, 347–361.